QED RADIATIVE CORRECTIONS IN DEEP INELASTIC NEUTRAL CURRENT ep SCATTERING: MONTE CARLO TREATMENT*

W. PŁACZEK

Institute of Physics, Jagellonian University
Reymonta 4, 30-059 Kraków, Poland

(Received April 27, 1993)

We describe two Monte Carlo algorithms for simulation of QED radiative processes in deep inelastic $e^{\pm}p \to e^{\pm}X$ scattering. One of them, implemented in the program LESKO-F, includes $\mathcal{O}(\alpha)$ QED radiative corrections. The other one describes multiphoton leptonic radiation in a framework of the Yennie–Frautschi–Suura exclusive exponentiation procedure and is a base of the program LESKO-YFS. Some numerical results of the above Monte Carlo programs are presented. We also comment on including QCD effects and hadronization in the both programs. Next, we discuss a problem of unfolding QED radiative corrections from the data. We present two methods of reducing hard photon radiation effects in the low x region. In one of them tagging hard radiative photons almost collinear with the incident electrons is used to estimate a non-radiative cross section. Experimental aspects of photon tagging are also discussed. The other method exploits information from a measurement of both final state electron and hadrons energies and angles to tag and reject hard initial radiation photon events. Some toy models of electron and hadron detectors are considered in this study. Both methods allow to reduce significantly QED radiative effects and can be used to extract the proton structure function at HERA. Finally, we argue that an effect of a reduction of an effective electron beam energy due to hard initial state photon radiation can be used to measure the longitudinal structure function at HERA. Results of a Monte Carlo simulation including statistical accuracy and systematic effects are presented.

PACS numbers: 11.40. Ks, 13.60. Hb, 02.70. Lq

---

* Work partly supported by the Polish Government grants KBN 2 2372 91 02 and 2 0380 91 01.

1. Introduction

High energy lepton scattering has been crucial in the development of our understanding of nature. Starting from J.J. Thompson's discovery of the electron [1], and Roentgen's discovery of X-Rays [2], *via* atomic energy quantization by Frank and Hertz in 1914 [3], to wave-particle duality in the interference experiments of Davison and Germer in 1927 [4] and the establishment of quantum mechanics. Subsequently the first precision measurement of the charge radius of atomic nuclei by Hofstadter in the late 1950s [5], the observation of scale invariance in the deep inelastic fragmentation of the proton at SLAC in 1970 [6], its interpretation in terms of quasi-free parton constituents by Feynman [7], the first direct observation of electroweak phenomena in the form of the observation of weak neutral currents [8], asymptotically free QCD motivated by the observation of scaling violation in deep inelastic lepton scattering in the 1970s [9], have all shaped the form of modern particle physics. The large storage ring HERA (Hadron-Electron-Ring-Anlage), which has been completed at DESY in early 1992, is supposed to be the next significant step on this way. It is the first electron proton storage ring ever built. Electrons and protons of nominal energies $E_e = 30\,\mathrm{GeV}$ and $E_p = 820\,\mathrm{GeV}$ collide head on. The centre of mass energy is $\sqrt{s} = \sqrt{4E_eE_p} \approx 314\,\mathrm{GeV}$. This is equivalent to an electron beam of 51 TeV incident on a stationary target. The beam energies can be varied within the following limits: $E_e = 10-35\,\mathrm{GeV}$ and $E_p = 300-1000\,\mathrm{GeV}$. The design luminosity is $1.5 \cdot 10^{31}\,\mathrm{cm}^{-2}\mathrm{s}^{-1}$. The total luminosity accumulated per year could thus reach $100\,\mathrm{pb}^{-1}$. HERA is also designed to produce longitudinally polarized electron or positron beams. A very detailed discussion of physics expected at HERA can be found in Refs [10] and [11].

One of the most promising possibilities offered by HERA is a measurement of the proton structure functions in completely new kinematical regions. Such a measurement can be performed with respect to the Bjorken scaling variable x down to $x \approx 10^{-4}$ and with respect to the momentum transfer Q^2 up to $Q^2 \approx 4 \cdot 10^4\,\mathrm{GeV}^2$. A great interest focuses on the low x ($x \leq 10^{-2}$) region, where some new phenomena may appear [12, 13].

QED radiative corrections are well known to be a reason of significant distortions in distributions of observed physical quantities in high energy physics experiments. This phenomenon was seen in older deep inelastic experiments [14], and the corresponding QED corrections for HERA were estimated first in Ref. [15]. The complete $\mathcal{O}(\alpha)$ electromagnetic and weak corrections have been calculated independently in Refs [16, 17] and in Refs [18, 19], see also Ref. [20]. In both approaches bremsstrahlung photon is treated totally inclusively and cross sections are calculated from initial and final lepton momenta only. Similar calculations were performed in the leading logarithmic approximation [21–24]. All they show that radiative correc-

tions in deep inelastic *ep* neutral current scattering at HERA are large, even of order of 100% and more, when cross-sections are evaluated only from the lepton momenta. They are dominated by QED bremsstrahlung from the lepton line and vacuum polarization corrections to the photon propagator [25, 26]. While vacuum polarization corrections, in principle, are rather easy to estimate (they enter into normalization), the bremsstrahlung contributions depend strongly on the experimental (complicated) set-up (cuts, angular detector coverages, selection criteria, resolutions, *etc.*). Furthermore, at HERA they may depend significantly upon an assumed shape of the structure functions in the kinematical domain that has not been explored by the previous experiments [27]. It is impossible to implement all those complicated assumptions in an analytical calculation. The only tool that is able to deal with them is *Monte Carlo event generator* which simulates *ep* scattering process directly.

Monte Carlo (M.C.) techniques have proved to be a valuable and even indispensable tool in high energy physics experiments. Monte Carlo event generators are used to simulate explored physical processes and their detection both at the stage of the planning of the experiment and in the actual analysis of experimental data. In general, Monte Carlo generators can be divided into two classes: (1) event generators simulating physical processes (based on theory) and (2) detector simulation programs which model detector behaviour. The former ones are plugged in as a first step in (usually larger) detector simulation programs. Also additional event selection criteria used in the data analysis (all sorts of cuts, triggers) can be introduced in the M.C. simulation in the same way as in the real data analysis, *i.e.* by rejecting some of the M.C. events.

The first M.C. event generator for a study of radiative correction in deep inelastic *ep* scattering at HERA, called LESKO-C, was written by Jadach in 1986 [21]. This program, based on the initial collinear bremsstrahlung approximation from the lepton line, was used in the analysis of the influence of QED radiative corrections on the data for the HERA Workshop 1987 [10], see *e.g.* [28]. LESKO-C became also the starting-point for developing the program LESKO-F [29] which includes the whole $\mathcal{O}(\alpha)$ QED bremsstrahlung from the lepton line. The program allows for a nonzero lepton beam polarization and apart from bremsstrahlung it takes into account the vacuum polarization corrections. The non-deep inelastic region (low Q^2) is excluded from an event generation by imposing a lower cut-off of the hadronic transverse momentum p_T. It ensures that the transfer momentum squared Q^2 is greater than some $Q^2_{\min} \approx p^2_{T,\min}$ (the program allows also to impose the cut $Q^2_{\min}$ directly). The p_T-cut seems to be a natural trigger for deep inelastic events in a real experiment [28]. Such a trigger is especially desirable in the presence of leptonic bremsstrahlung when the true Q^2 may

be much lower than one obtained from the lepton momenta. Implementation of such a cut-off in the very early stage of the M.C. program improves significantly an efficiency of event generation. At present, there is available another version of the LESKO program, called LESKO-YFS [30], which incorporates multiphoton radiation from the lepton line. It is based on the Yennie, Frautschi and Suura exclusive exponentiation procedure [31].

The M.C. algorithm implemented in the above programs may be characterized as *an individually adapted Monte Carlo (IAMC) algorithm* [32]. the main feature of IAMC algorithms is that they are constructed and optimized individually for a given process. They are based on a detailed knowledge of generated distributions and therefore they are usually much more efficient than ones employing general purpose generation procedures.

Both LESKO-F and LESKO-YFS simulate the *ep* deep inelastic scattering in the framework of the quark–parton model. The hadronic part is described in terms of parton distribution functions. The above programs provide the hadronic final state at the parton level. Parton fragmentation can be done, however, with the help of the program FRANEQ [33], which interfaces both LESKO-F and LESKO-YFS with hadronization routines from the Lund programs LEPTO 5.2 [34] and JETSET 6.3 [35]. It also includes QCD radiative processes described in the framework of the parton shower picture.

Other M.C. programs for the HERA purpose including radiative corrections are: HERACLES by Kwiatkowski, Möhring and Spiesberger [36] and KRONOS by Anlauf *et al.* [37]. The program HERACLES is based on the calculations of the $\mathcal{O}(\alpha)$ order electroweak radiative corrections of Refs [18, 19] and employs the Monte Carlo integration algorithm VEGAS by P. Lepage [38]. The event generator KRONOS includes higher order QED radiative effects in the leading logarithmic approximation. It is based on the M.C. algorithm for parton cascades as it is done for quark fragmentation in QCD [35].

As it has been mentioned above, QED radiative corrections will strongly distort the distributions of the observed quantities at HERA. Their size depends in the complicated way on the experimental conditions, such as triggers, cuts, angular detector coverages, detector resolutions, capacities of the exclusive measurement, *etc.* All those requirements can be fulfilled only by the use of the Monte Carlo simulation methods. An effective M.C. event generator is, therefore, a very helpful tool for an analysis of radiative corrections under the realistic experimental conditions. It can also be used to work out efficient methods of eliminating radiative effects from the data. With the help of the program LESKO-F two methods of reducing radiative effects at HERA were developed and tested. The first one is based on the leptonic momenta measurement and tagging part of the hard radiative pho-

tons by means of the luminosity monitors. The method has been proposed in Ref. [39], whereas in Ref. [40] it has been checked against the realistic experimental conditions. In the second method, proposed in Ref. [41], the QED effects are significantly reduced when the simultaneous measurement of the leptonic momenta and the longitudinal hadronic energy flow is performed and some rejecting conditions are applied. It was tested with the help of the program FRANEQ including QCD effects and using toy models of the detectors.

In contrast to the above methods, where the QED radiative effects are eliminated from the data, in Ref. [42] we propose a method in which they can be utilized to extract some physically important information. The emission of the photons collinear to the incident lepton leads to a reduction of the effective beam energy. This effect is proposed to be used to measure the longitudinal structure function at HERA. The method has been analysed and tested with the help of the programs LESKO-C and LESKO-F.

This work, in general, is based on Refs [29, 33, 39–42], but we do not attempt to reproduce all the results of the above papers. We rather concentrate recalling the main points of these references, drawing up essential conclusions as well as discussing those topics which were not fully covered in these papers. A completely new topic introduced in this work is the implementation of the Yennie–Frautschi–Suura exponentiation in the M.C. simulation of deep inelastic *ep* scattering.

The outline of the article is the following. In Subsection 1.1 we give the lowest order formula for deep inelastic lepton proton scattering. The problem of radiative corrections is discussed in Subsection 1.2. Section 2 contains descriptions of the Monte Carlo algorithms employed in both LESKO-F (Subsection 2.1) and LESKO-YFS (Subsection 2.2) programs, some numerical results obtained from those programs (Subsection 2.3), and finally some details on including QCD effects and hadronization (Subsection 2.4). In Section 3 we discuss the unfolding procedures for radiative corrections at HERA, while in Section 4 we describe the method of determining the longitudinal structure function from the radiative events, and Section 5 summarizes this work.

1.1. Cross section and structure functions

The lowest order deep inelastic neutral current scattering process

$$l(p_1) + p(P) \longrightarrow l(p_2) + X(p_X), \quad l = e^{\pm}, \tag{1}$$

where l denotes electron or positron, p proton and X a hadronic final state, is illustrated in Fig. 1(a).

For the overall event kinematics there are only two independent variables and thus measuring the energy (E_2) and the angle (θ_2 — with respect

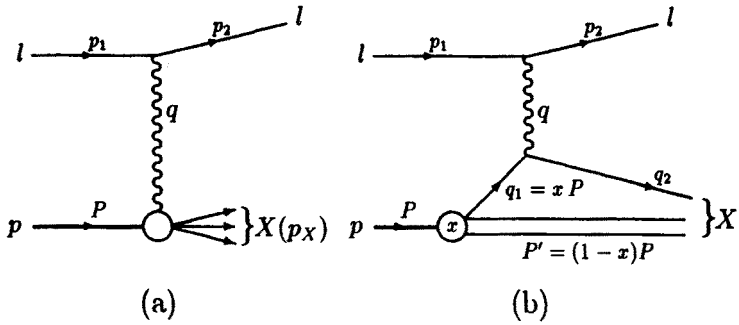

Fig. 1. Basic diagrams for deep inelastic lepton proton neutral current scattering: (a) in general, without assumption about the structure of the initial proton and the final hadronic system, and (b) in the quark–parton model.

to the incident lepton beam) of the scattered lepton, all other variables can be calculated. The total center mass energy squared is

$$s_0 \equiv (p_1 + P)^2 \simeq 4E_1E_p\,. \tag{2}$$

In the neutral current processes the interaction is mediated by vector bosons γ or Z which carry the space-like four-momentum $q = p_1 - p_2$. We define the momentum transfer variable Q^2,

$$Q^2 \equiv -q^2 = -(p_1 - p_2)^2 \simeq 4E_1E_2\sin^2\frac{\theta_2}{2}\,, \tag{3}$$

which obviously is positive. The commonly used scaling variables, Bjorken-x and y, are defined as follows

$$x \equiv \frac{Q^2}{2P\cdot q} \simeq \frac{E_1E_2\sin^2\frac{\theta_2}{2}}{E_p(E_1 - E_2\cos^2\frac{\theta_2}{2})}\,, \tag{4}$$

$$y \equiv \frac{P\cdot q}{P\cdot p_e} = \frac{2P\cdot q}{s_0} \simeq \frac{E_1 - E_2\cos^2\frac{\theta_2}{2}}{E_1}\,. \tag{5}$$

It is obvious from the above definitions that these variables are always in the range $0 \le (x, y) \le 1$. Finally we define the invariant mass W of the hadronic final state

$$W^2 \equiv (q + P)^2 = Q^2\frac{1-x}{x} + m_p^2\,, \tag{6}$$

where m_p is the proton mass. This variable is important for hadronization. Since for the fixed energies of the incident beams there are only two degrees

of freedom, for description of the process (1) one may use only two of the above variables. The most commonly used pairs are (x, Q^2) and (x, y).

Within the quark-parton model, where the proton is composed of almost free partons (quarks and gluons), the deep inelastic *ep* scattering process is described through elastic scattering of electron on quarks, Fig. 1(b). In this picture the Bjorken scaling variable x can be interpreted as a fraction of the proton momentum which is carried by the struck quark before the interaction. This picture is not valid when QCD corrections are taken into account.

The differential cross section for the process (1) can be written as follows

$$\frac{d^2\sigma^{\pm}_{NC}}{dx\,dQ^2} = \frac{2\pi\alpha^2}{xyQ^2}[Y_+\mathcal{F}_2(x,Q^2) \mp Y_- x\mathcal{F}_3(x,Q^2) - y^2\mathcal{F}_{\rm L}(x,Q^2)]\,, \qquad (7)$$

where

$$Y_\pm = 1 \pm (1-y)^2\,, \qquad (8)$$

and

$$\mathcal{F}_{\rm L}(x,Q^2) = \mathcal{F}_2(x,Q^2) - 2x\mathcal{F}_1(x,Q^2)\,. \qquad (9)$$

The form-factors $\mathcal{F}_1$, $\mathcal{F}_2$, $\mathcal{F}_3$, $\mathcal{F}_{\rm L}$ are the structure functions of the proton. If only γ exchange is assumed then they are equal to the conventional electromagnetic structure functions F_1, F_2, F_3, $F_{\rm L}$ (this is good approximation for low Q^2, and hence low x). The structure functions of Eq. (7) include electroweak coupling constants and the lepton polarization. They can be evolved as follows

$$\mathcal{F}_{1,2} = \sum_{i,j=\gamma,Z} \chi^i(Q^2)\chi^j(Q^2)(\lambda_{\rm V}^{eij} - P_{\rm L}\lambda_{\rm A}^{eij})F_{1,2}^{ij}\,, \qquad (10)$$

$$\mathcal{F}_3 = \sum_{i,j=\gamma,Z} \chi^i(Q^2)\chi^j(Q^2)(\lambda_{\rm A}^{eij} - P_{\rm L}\lambda_{\rm V}^{eij})F_3^{ij}\,, \qquad (11)$$

where $P_{\rm L}$ is the degree of longitudinal polarization of the lepton, and

$$\chi^\gamma = 1\,, \qquad \chi^Z(Q^2) = \frac{Q^2}{Q^2 + M_Z^2}\,. \qquad (12)$$

The electroweak coupling constants

$$\lambda_{\rm V}^{fij} = v_f^i v_f^j + a_f^i a_f^j\,,$$
$$\lambda_{\rm A}^{fij} = v_f^i a_f^j + a_f^i v_f^j\,, \qquad (13)$$

are expressed in terms of the vector and axial coupling constants v_f^i and a_f^i of the fermion f to the neutral currents

$$v_f^\gamma = -Q_f\,, \quad v_f^Z = \frac{I_3^f - 2s_W^2 Q_f}{2s_W c_W}\,,$$
$$a_f^\gamma = 0\,, \qquad a_f^Z = \frac{I_3^f}{2s_W c_W}\,, \tag{14}$$

where Q_f is the charge of the fermion f and I_3^f its third isospin component while $s_W = \sin\theta_W$, $c_W = \cos\theta_W$, and θ_W is the weak mixing angle [43] which is determined by the gauge bosons masses

$$c_W = \cos\theta_W = \frac{M_W}{M_Z}\,. \tag{15}$$

As long as the W boson mass is not very precisely known, it is better to parametrize the Z coupling constants in terms of the μ decay constant G_μ [44]:

$$s_W^2 c_W^2 = \frac{\pi\alpha}{\sqrt{2}G_\mu M_Z^2}\,\frac{1}{1-\Delta r}\,, \tag{16}$$

where Δr includes higher order corrections (in the lowest order expression $\Delta r = 0$).

In the quark–parton model, Fig. 1(b), the proton structure functions can be expressed through quark distribution functions

$$F_2^{ij}(x,Q^2) = x\sum_f [q_f(x,Q^2) + \bar{q}_f(x,Q^2)]\lambda_{\mathrm{V}}^{fij}\,, \tag{17}$$

$$F_3^{ij}(x,Q^2) = \sum_f [q_f(x,Q^2) - \bar{q}_f(x,Q^2)]\lambda_{\mathrm{A}}^{fij}\,. \tag{18}$$

From the Callan–Gross relation [45], $2xF_1 = F_2$, which holds for massless spin 1/2 partons with zero transverse momenta, the longitudinal structure function vanishes

$$\mathcal{F}_{\mathrm{L}}(x,Q^2) = 0\,. \tag{19}$$

The above relation is violated by QCD effects[1], which make $\mathcal{F}_{\mathrm{L}}$ nonzero and proportional to α_s. This can be neglected to a good approximation except the very low x region. At the low x region the longitudinal structure function is dominated by the contribution from gluons and its measurement can be used for the extraction of the gluon distribution function [46].

[1] It remains valid still in the QCD leading logarithmic approximation.

1.2. Radiative corrections

The formulae in the previous Subsection are given at so called "tree level", *i.e.* they do not include quantum effects[2]. The quantum effects, usually called radiative corrections, which enter the formula for the cross section can originate from both electroweak and strong interactions. In this paper we do not deal with QCD (strong interactions) effects, however some remarks on this point we give in Subsection 2.4. Electroweak radiative corrections in deep inelastic *ep* scattering can be calculated on a perturbative way (order by order) in the framework of the Standard Model for electroweak interactions [43] following Feynman diagrams rules. The perturbative series is, in such an approach, expanded with respect to the fine coupling constant α. Corrections $\mathcal{O}(\alpha)$ are usually calculated first. It seems to be justified since the fine structure constant is numerically small ($\alpha \simeq 1/137$) and higher order corrections are expected to be small. Various kinematic effects may, however, cause that certain classes of radiative corrections are numerically much more significant than others, and that even higher orders corrections are important.

As it was mentioned in the Introduction, the $\mathcal{O}(\alpha)$ electroweak radiative corrections at HERA are dominated by QED effects. Genuine weak corrections, *i.e.* without the vacuum polarization, reach maximally 2% [26]. Then, among QED corrections, the most significant in the wide range of the kinematical domain is bremsstrahlung from the lepton line. It may reach even 100% or more in the region of low x and high y [16, 18, 26, 27]. The size of this effect can be reduced by the simultaneous measurement of leptonic and hadronic momenta, but, unfortunately, it is not possible experimentally in the whole kinematical domain, particularly in the low-x range — where corrections are the biggest! The similar correction to the quark line is much less important. Its leading logarithmic terms can be absorbed into the proton structure function likewise as QCD effects [47, 48]. The remaining non-leading corrections are negligible if an experimental accuracy is not better than 1% order [25, 26]. The second numerically significant correction is one due to the vacuum polarization. It modifies the exchanged photon propagator and can be taken into account by the use of the running fine structure constant (or the effective fine structure constant)

$$\alpha(Q^2) = \frac{\alpha(0)}{1 - \Pi_{\gamma\gamma}(Q^2)} \,. \tag{20}$$

---

[2] In fact, they include leading QCD effects absorbed into the hadronic structure functions which, as a consequence, feature scaling violation behaviour (Q^2 dependence).

It includes contributions from all possible particles that couple to the photon, but practically is dominated by fermion loops. While the leptonic contribution can be calculated analytically [49], the hadronic one has to be taken from the experiment via dispersion relations [50]. At $Q^2 = M_Z^2$ the value of $\Pi_{\gamma\gamma}$ is about 0.06.

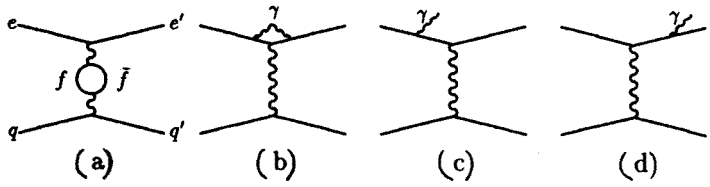

Fig. 2. Diagrams for numerically most important $\mathcal{O}(\alpha)$ radiative corrections at HERA: a) the vacuum polarization, b) the photon lepton vertex correction, c) and d) real photon radiation from the initial and final lepton states, respectively.

It has been shown that for the accuracy of a few % it is sufficient to take into account the leptonic QED corrections and the vacuum polarization functions as in Eq. (20) [25, 26]. Diagrams for these processes are presented in Fig. 2. The diagram in Fig. 2a represents the vacuum polarization. The bremsstrahlung processes with the additional photon in the final state are represented by the diagrams in Figs. 2c, d. In the calculation of the cross section they have to be combined with virtual photonic correction to the vertex function, Fig. 2b, in order to cancel the infrared singularity. To ensure gauge invariance the contributions of the diagrams in Figs. 2c and 2d have to summed and squared. It is not possible to treat the initial and final state radiation separately because of the interference terms which also contribute to the cross section. Classification of bremsstrahlung as radiation from the initial or final states has only conventional meaning. It can be done by looking at the photon emission direction. Theoretically, such a distinction is meaningful in the leading logarithmic approximation only.

The most recent review of radiative corrections at HERA as well as presentation of programs for calculating them can be found in Ref. [26]. The magnitude of the first order leptonic bremsstrahlung corrections indicates that higer orders may also be significant. Including higher order contributions following the Feynman diagram rules is usually rather difficult. Because of this it is profitable to exploit certain approximations. One of them is the leading logarithmic approximation. In this approach one takes into account only leading logarithmic terms $\sim \ln(Q^2/m_l^2)$ corresponding collinear peaks in the photon–fermion angle. It is possible to sum those terms even up to the infinite order. A recent excellent review of leading logarithmic calculations for QED one can find in Ref. [51]. In

such calculations one misses all subleading terms which may, however, give a non-negligible contribution. The second order leading logarithmic QED corrections at HERA was calculated in Ref. [52]. It has been shown that they are generally small, except the low x and high y region.

Another approach to QED calculations is so called *exponentiation.* A strict and physically well founded prescription for exponentiation was proposed by Yennie, Frautschi and Suura in their classical work of Ref. [31]. The main idea of this scheme is to rearrange the entire QED perturbative series of any process in such a way that the infrared (IR) singularities are factored out, summed up to the infinity and properly canceled. The remaining, not exponentiated, IR finite series can be calculated perturbatively (exactly or in the leading logarithmic approximation). This procedure, usually called the exclusive YFS exponentiation, offers a well defined recipe for Monte Carlo applications. It has been extensively used for M.C. simulation of the e^+e^- processes at LEP/SLC, see Refs [53, 54] and references therein. It has been shown that the exclusive YFS exponentiation is the most effective way of including higher order effects and it offers a faster improvement of an accuracy than traditional QED calculations (order by order) [51, 55].

2. Monte Carlo simulation of QED effects

In this Section we shall present the Monte Carlo algorithms implemented in two programs for simulation of deep inelastic scattering at HERA including QED radiative corrections. The first one, implemented in the program LESKO-F, is based on the exact $\mathcal{O}(\alpha)$ calculation for QED leptonic bremsstrahlung and the other one, implemented in the program LESKO--YFS, simulates multiphoton radiation from the lepton line according to the exclusive YFS exponentiation procedure [31] in the $\mathcal{O}(\alpha)$. We are not going to describe a general framework of the Monte Carlo techniques, this is beyond the scope of this paper. The readers interested in this subject we can refer *e.g.* to Refs [56, 32, 57]. Both M.C. algorithms to be presented are individually adapted to the undertaken processes, *i.e.* they take into consideration specific features of these processes. Such an approach in constructing the M.C. generators provides the most effective solutions of the simulation problems.

Random numbers needed in the M.C. simulation are generated in both programs by the use of the switchable generator VARRAN which chooses among two good quality random number generators RANMAR [58] and RANECU [59]. The algorithms of the programs LESKO-F and LESKO--YFS are built on the base of the differential cross sections for deep inelastic neutral current ep scattering including appropriate QED corrections. The event generation is steered through a set of input parameters which

have to be set up before running the program. In general, the programs run in three steps — all of them in a single task. In the first step (initialization mode) the input data are transferred to the program through the steering parameters; it is obligatory. In the second step (event generation mode) a M.C. event is produced according to the employed M.C. algorithm. Each event is expressed in terms of flavours and four-momenta of final particles at the parton level (hadronization is not performed). The third step (post-generation mode — optional) terminates generation and provides some useful output corresponding to a generated sample. The programs LESKO-F and LESKO-YFS are restricted to the deep inelastic scattering domain by introducing low Q^2 region cuts. They allow to chose among two triggers, the minimum of the momentum transfer $Q^2_{\min}$ and the minimum of the hadronic transverse momentum $p_{\mathrm{T,min}}$. The latter is more convenient from experimental point of view. It ensures that $Q^2 > p^2_{\mathrm{T,min}}$ even in the presence of leptonic photon radiation. The hadronic part of the process is described with the help of the parton distribution functions which have a scaling violation behaviour, *i.e.* they include leading QCD effects. The programs are interfaced with a large package of older and recent parton distribution functions parametrizations, called PAKPDF [60]. More details about them one can find in Ref. [60] and references therein. The parametrizations of the parton distribution functions are provided to the programs through external routines, so they can be easily replaced by any other ones. The programs can produce both weighted and unweighted ($w = 1$) events according to the option chosen by the user.

2.1. Single leptonic bremsstrahlung

The program LESKO-F simulates the deep inelastic neutral current electron scattering process which includes the single photon radiation from both the initial and final states. The kinematics for the process

$$l(p_1) + p(P) \longrightarrow l(p_2) + \gamma(k) + X(P'), \quad l = e^{\pm}, \tag{21}$$

is schematically depicted in Fig. 3.

The process (21) is described within the quark–parton model, *i.e.* the incoming lepton l scatters on the point-like quark inside the proton which carries the four-momentum $q_1 = xP$, where x is the Bjorken scaling variable. After the collision, which is mediated by the electroweak neutral bosons (γ and Z) with the space-like momentum q, the outgoing quark has the four-momentum q_2. The rest of the proton (proton remnant), which is not scattered, has the four-momentum $P' = (1 - x)P$. The bremsstrahlung photon γ emitted in the scattering process from the incoming/outgoing leptons carries the four-momentum k.

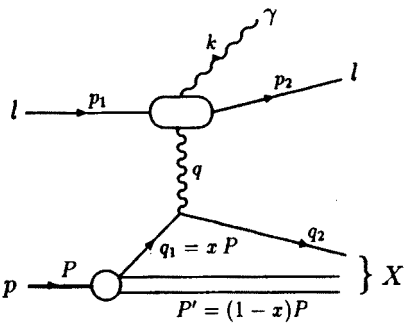

Fig. 3. The kinematics of the deep inelastic neutral current electron–proton scattering process including single photon bremsstrahlung from the lepton line.

Apart from the $\mathcal{O}(\alpha)$ leptonic bremsstrahlung the program includes also the vacuum polarization correction and the correction Δr to the muon decay constant [44]. The latter is used for calculation of the weak coupling constants. The program LESKO-F is described in detail in Ref. [29]. In this section we shall present the main points of the Monte Carlo algorithm employed in LESKO-F. The recent version of the program, unlike the previous ones, gives the possibility to generate weighted events, not only events with the constant weight, $w = 1$.

The total cross section for the process (21) can be expressed in the following compact form:

$$\sigma = \int\limits_{|t|_{\min}}^{s_0} d\,|\,t\,| \int\limits_0^1 dx \int\limits_0^{2\pi} \frac{d\phi}{2\pi} \int\limits_0^1 dz_1 \int\limits_0^1 dz_2 \int\limits_0^{2\pi} \frac{d\psi}{2\pi}\, \varrho(t, x, z_1, z_2, \phi, \psi)\,,$$

$$\varrho(t, x, z_1, z_2, \phi, \psi) = \sum_q q_q(x, t)\, \rho_q(t, x, z_1, z_2, \phi, \psi)\, \Xi_{\mathrm{MC}}(p_2, q_2, k)\,, \quad (22)$$

$$s_0 = (p_1 + P)^2\,, \quad s = (p_1 + q_1)^2\,, \quad s_1 = (p_2 + q_2)^2\,,$$
$$t = q^2 = -Q^2 = (p_1 - p_2 - k)^2\,, \quad p_1^2 = p_2^2 = m_l^2\,, \quad q_2^2 = m_q^2\,, \quad (23)$$

where $\rho_q(t, x, z_1, z_2, \phi, \psi)$ is the differential cross section of the lepton–quark (lq) scattering including the single photon emission from the lepton line; the index q denotes the quark flavour.

The variable ϕ in formula (22) is a trivial azimuthal angle around the beam ($+z$ axis along the electron direction) and ψ is the azimuthal angle defined in the rest frame of $(p_2 + k)$ with respect to the plane defined by the incoming electron and outgoing quark momenta $(\vec{p_1}, \vec{q_2})$ with the third axis pointing in direction of the incoming electron.

The last two variables used in the above formula are defined as follows

$$z_1 = \frac{2(kp_1)}{|t| + 2(kp_2)}, \qquad z_2 = \frac{2(kp_2)}{|t| + 2(kp_2)}. \tag{24}$$

The area covered by these variables almost coincides with the unit square $0 \leq z_i \leq 1$. More precisely, the z-variables satisfy the conditions

$$\delta_1(z_2) \leq z_1 \leq 1, \qquad \delta_2(z_1) \leq z_2 \leq 1, \tag{25}$$

where

$$\delta_1(z_2) = \frac{m_l^2}{|t|} z_2(1 - z_2), \qquad \delta_2(z_1) = \frac{m_l^2}{|t|} \frac{z_1}{1 - z_1}. \tag{26}$$

The essential property of the z-variables is that they have a rather simple meaning for hard collinear photon emission. For hard collinear emission from the initial electron state, z_2 is simply *the fraction of the incoming electron momentum carried by a hard collinear photon* ($z_1 \approx 0$). While for hard collinear emission from the final electron state z_1 is *the fraction of the momentum of the dissociating quasi-real electron carried by a hard collinear photon* ($z_2 \approx 0$).

The function $q_q(x,t)$ in formula (22) is a distribution of the quark q inside the proton. The program allows to use various parametrizations for the quark distribution functions, *e.g.* those collected in the package PAKPDF described in Ref. [60].

The function $\Xi_{\rm MC}(p_2, q_2, k)$ in formula (22) imposes the trigger conditions (defines the available phase space) used in the M.C. generation. The present version of the program includes two options for DIS trigger:

$$\Xi_{\rm MC} = \Theta(p_{\rm T} - p_{\rm T,min}) \tag{27}$$

and

$$\widetilde{\Xi}_{\rm MC} = \Theta(|t| - |t|_{\rm min}). \tag{28}$$

The former corresponds to the lower cut of the final hadronic (quark) transverse momentum (in our case $p_{\rm T}^2 = (q_2^1)^2 + (q_2^2)^2$) while the latter to the lower cut of the "true" Q^2 (*i.e.* on the hadronic side). The recent version allows also to impose additional lower and upper cuts on the hadronic x, Q^2, y. Any other user's own trigger $\Xi_{\rm exp}$ can be simulated by rejecting some generated events.

From now on we always assume $p_1^2 = p_2^2 = m_l^2 = m^2 \ll |t|$ and $q_1^2 = q_2^2 = 0$. The differential cross section ρ_q of Eq. (22) is divided, as usual, into two parts corresponding to soft and hard photon radiation.

$$\rho_q(t, x, z_1, z_2, \phi, \psi) = \delta(z_1)\,\delta(z_2)\,\rho_q^{\rm soft}(t, x, \phi, \psi; \Sigma) + \Theta(z_1/\epsilon_1 + z_2/\epsilon_2 - 1)\,\rho_q^{\rm hard}(t, x, z_1, z_2, \phi, \psi), \tag{29}$$

where Σ, defined by

$$\frac{z_1}{\epsilon_1} + \frac{z_2}{\epsilon_2} < 1\,, \tag{30}$$

is a boundary between the soft and hard bremsstrahlung regions. The infrared singularity (for $z_1 = z_2 = 0$) is cancelled in the standard way by adding the virtual photon contribution from the vertex function (regularized by a finite photon mass) inside the boundary Σ. The boundary Σ which splits the phase space into the soft and hard bremsstrahlung regions is defined in terms of the z-variables. Such an approach is much more useful for our M.C. algorithm than the traditional way of imposing this cut in the laboratory frame on the photon energy E_γ. Our boundary must, however, satisfy the condition that in the "soft" region ($z_1/\epsilon_1 + z_2/\epsilon_2 < 1$) radiative photons have the energy below some value $E_\gamma^{\min}$, which should be as small as possible. Smallness of $E_\gamma^{\min}$ is required both by a reliability of the soft photon approximation and by experimental resolution criteria ($E_\gamma^{\min}$ should lie below the experimental threshold $E_{\exp}^{\min}$). On the other hand, if $E_\gamma^{\min}$ is too small, the "soft" contribution ρ_q^{soft} in (29) might become negative, which is not convenient in the M.C. algorithm. In general, it is possible to use in the M.C. simulation negative distributions, but in such a case generated events have to be weighted with the appropriate negative weight. It is impossible, however, to turn those variable-weight events into more useful constant-weight events. Therefore, one should take care for $\rho_q^{\text{soft}}(\Sigma)$ to be positive[3]. We have found that the choice of Σ with $\epsilon_1 = 10^{-4}$ and $\epsilon_2 = 10^{-3}$ is acceptable for HERA. For the above boundary radiative photons with the energy above $\simeq 0.05$ GeV are not distorted by the "soft" cut. Although the "soft" and "hard" contributions to the cross section separately depend on the choice of the boundary Σ, their sum should not depend on it. With help of the M.C. exercise we checked that the program fulfils this requirement for the wide range: $10^{-4} \leq \epsilon_1 \leq 10^{-2}$ and $10^{-3} \leq \epsilon_2 \leq 10^{-2}$.

The "soft" part can be calculated analytically and it reads

$$\begin{aligned} \rho_q^{\text{soft}}(t, x, \phi, \psi; \Sigma) &= D_{lq}(s,t)\, \Delta^{\text{soft}}(t; \Sigma)\,, \\ \Delta^{\text{soft}}(t; \Sigma) &= 2\pi\, \delta(\psi)\,(1 + \delta_{\text{soft}}(\Sigma))\,, \end{aligned} \tag{31}$$

where

$$\delta_{\text{soft}}(\Sigma) = \frac{\alpha}{\pi}\left\{\left(\ln\frac{|t|}{m^2} - 1\right)\ln(\epsilon_1\epsilon_2) + \tfrac{3}{2}\ln\frac{|t|}{m^2} - \frac{1}{2}\ln^2\frac{\epsilon_1}{\epsilon_2} - \frac{\pi^2}{6} - 2\right\} \tag{32}$$

[3] The real solution for the problem with the choice of the boundary Σ is to avoid it by exponentiation [31].

$D_{lq}(s,t)$ in (31) is the differential cross section $d\sigma(s,t)/dt$ for lepton–quark scattering ($s = s_0 x$), given explicitly in Appendix A.

The "hard" part of the cross section can be expressed as follows

$$\rho_q^{\text{hard}}(t, x, z_1, z_2, \phi, \psi) = \frac{\pi^4}{2} \frac{|t|}{s^2(1-z_2)^2} |\mathcal{M}_q^{\text{hard}}|^2 \times \Theta(z_1 - \delta_1(z_2))\,\Theta(z_2 - \delta_2(z_1)), \qquad (33)$$

where $|\mathcal{M}_q^{\text{hard}}|$ is the matrix element of the lepton-quark neutral current scattering with the single hard photon emission from the lepton line; it is given explicitly in Appendix A.

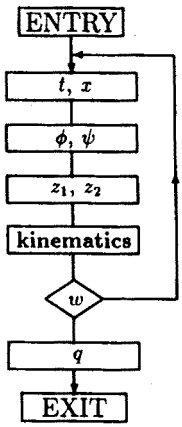

Fig. 4. Scheme of the Monte Carlo algorithm. Generation of the indicated variables and other operations are depicted by boxes and the return loop represents rejection of events (in the case of unweighted event generation).

Having defined all the ingredients in the master formula (22) we can now describe in more details the M.C. algorithm used to generate the differential distribution ρ. A schematic diagram of this algorithm is depicted in Fig. 4. The variables t, x, z_1, z_2, ϕ, ψ and the type of the scattered quark q are generated from top to bottom of the diagram. The return loop in this picture represents the rejection procedure in the M.C. algorithm in the case of unweighted event generation. In the case of weighted event generation there is no rejection and each event is accompanied with the appropriate weight w. If one wants to have results of the M.C. program in terms of "physical" events, one has to use the rejection technique which provides unweighted events ($w = 1$). The rejection technique, in general, consists in

replacing the distribution ϱ to be generated by the distribution ϱ_1 which is simpler than ϱ and therefore easier to generate. The "crude" distribution ϱ_1 ought to be as close as possible to ϱ. In the first step we generate the distribution ϱ_1 and for each event we calculate the weight $w = \varrho/\varrho_1$. This weight is then compared in the next step with a random number $r \in (0,1)$ and if $r \leq w$ the event is accepted, otherwise it is rejected and the procedure is repeated. This way, the accepted events are distributed according to the desired distribution ϱ and we deal with events with constant weight $w = 1$.

In order to obtain the distribution ϱ_1 we make two simplifications in the formula (22). First we perform the replacement

$$s_1 \longrightarrow s = s_0 x \,. \tag{34}$$

In such a case the function $\Xi_{\mathrm{MC}}(p_2, q_2, k)$ takes a simple form,

$$\Xi_{\mathrm{MC}}(p_2, q_2, k) \longrightarrow \Theta\left(x - \frac{s_{1,\min}(t)}{s_0}\right), \tag{35}$$

where

$$s_{1,\min}(t) = \frac{|\,t\,|^2}{|\,t\,| - p^2_{\mathrm{T},\min}} \,. \tag{36}$$

Apart from simplifying the distribution ϱ such a change enlarges somewhat the available phase space. Next, we replace the hard bremsstrahlung matrix element $\mathcal{M}_q^{\mathrm{hard}}$ by a new one which is much simpler for the M.C. generation, but, at the same time, close to the original one. The new distribution can be then written as

$$\varrho_1(t, x, z_1, z_2, \phi, \psi) = \kappa\Theta\left(x - \frac{s_{1,\min}(t)}{s_0}\right) \Delta(t, z_1, z_2) \sum_q D_{lq}(s_0 x, t) q_q(x, t), \tag{37}$$

where

$$\Delta(t, z_1, z_2) = \zeta(t, \Sigma) \Big\{ \delta(z_1)\,\delta(z_2)\,\Delta^{\mathrm{soft}}(t; \Sigma) + \Theta\left(\frac{z_1}{\epsilon_1} + \frac{z_2}{\epsilon_2} - 1\right) \Delta^{\mathrm{hard}}(t, z_1, z_2; \Sigma) \Big\} \tag{38}$$

and

$$\Delta^{\mathrm{hard}}(t, z_1, z_2; \Sigma) = \Theta(z_1 - \delta_1(z_2))\,\Theta(z_2 - \delta_2(z_1))\,\frac{\alpha}{\pi}\,\frac{1}{z_1 z_2}, \tag{39}$$

while $\Delta^{\text{soft}}(t;\Sigma)$ is defined in Eq. (31). The factor $\zeta(t,\Sigma)$ in Eq. (38) ensures that

$$\int_0^1 dz_1 \int_0^1 dz_2\, \Delta(t,z_1,z_2) = 1\,. \tag{40}$$

Due to the above nice feature of the function $\Delta(t,z_1,z_2)$ the variables (t,x) can be generated independently of (z_1,z_2). Thus, instead of the six-dimensional distribution ϱ we obtain a product of maximally two-dimensional distributions which can be generated independently of each other. From the integration in Eq. (38) over z_1 and z_2 we obtain the factor $\zeta(t,\Sigma)$ in the form

$$\begin{aligned}\zeta(t,\Sigma) &= \{\,1+\delta_{\text{int}}(t,\Sigma)\,\}^{-1}\,,\\ \delta_{\text{int}}(t,\Sigma) &= \frac{\alpha}{\pi}\left(\tfrac{3}{2}\ln\frac{|\,t\,|}{m^2} - \ln(\epsilon_1\epsilon_2) - 2\right).\end{aligned} \tag{41}$$

It is easy to check that at HERA energies and for our choice of the infrared boundary Σ: $\delta_{\text{int}} < 0.13$.

The generation of the variables used to parametrize the differential cross section is performed in the following way. The angles ϕ and ψ are chosen uniformly from the range $(0,2\pi)$. The variables (t,x) are generated according to the distribution

$$f(t,x) = \sum_q q_q(t,x)\, D_{lq}(s_0 x,t) \tag{42}$$

by the use of the two-dimensional M.C. sampler VESKO2, developed by S. Jadach [61]. This sampler at the first stage (initialization mode) sets up a grid of cells which is more dense in regions where $f(t,x)$ is higher and less dense in the rest of the integration domain. In a procedure of generating the pairs (t,x), first the cell is randomly chosen, and then the pair (t,x) is generated within the cell (by means of rejection) precisely according to the distribution $f(t,x)$. In order to eliminate from the generated distribution the leading singularity $x^{-1}(M^2-t)^{-2}$, where M is the exchanged boson mass ($M=0$ for γ), the following change of variables is done in the integration over t and x

$$\int_{|t|_{\min}}^{|t|_{\max}} d\,|\,t\,| \int_{x_{\min}}^{x_{\max}} dx\, f(t,x) = \int_0^1 d\alpha \int_0^1 d\beta\, g(\alpha,\beta)\,, \tag{43}$$

where

$$g(\alpha,\beta) = f(t,x)\, x \ln\left(\frac{x_{\max}}{x_{\min}}\right) \frac{(|t|+M^2)^2(|t|_{\max}-|t|_{\min})}{(|t|_{\max}+M^2)(|t|_{\min}+M^2)}, \quad (44)$$

$$|t| = \frac{(|t|_{\max}+M^2)(|t|_{\min}+M^2)}{|t|_{\max}+M^2-\alpha(|t|_{\max}-|t|_{\min})} - M^2, \quad (45)$$

$$x = x_{\min}^{1-\beta} x_{\max}^{\beta}. \quad (46)$$

Apart from removing the leading singularity of the integrand the new variables satisfy the requirement $\alpha, \beta \in (0,1)$ of the sampler VESKO2. At the final stage (post-generation mode) the sampler yields the value of the integral (43) with a good precision as well as its relative statistical error. These values are needed to evaluate the total cross section σ.

The values (z_1, z_2) are generated according to the distribution $\Delta(t, z_1, z_2)$ when t is already known. This generation is rather easy to perform by the use of simple M.C. methods as described in Ref. [32]; for detail we refer the reader to the source code of LESKO-F.

After generation of all the needed variables the weight w is calculated according to

$$w = \varrho(t, x, z_1, z_2, \phi, \psi)/\varrho_1(t, x, z_1, z_2, \phi, \psi). \quad (47)$$

The dummy parameter κ in the formula (37) is adjusted[4] such that $w \leq 1$. For the basic process (21), a numerical experiment or an inspection of relevant formulae shows that one can set $\kappa = 1.13$. The total cross section (22) can be estimated from the relation

$$\sigma = \sigma_1 \langle w \rangle, \quad (48)$$

where $\langle w \rangle$ is the average weight taken over all generated events[5]. The approximate cross section

$$\sigma_1 = \int d|t|\, dx\, dz_1\, dz_2\, d\phi\, d\psi\, \varrho_1(t, x, z_1, z_2, \phi, \psi)$$

$$= \kappa \int_{|t|_{\min}}^{s_0} d|t| \int_{s_{1,\min}/s_0}^{1} dx \sum_q q_q(t,x)\, D_{lq}(s_0 x, t) \Delta(t, z_1, z_2) \quad (49)$$

---

[4] The parameter κ is dummy, *i.e.* none of the numerical results should depend on it (within a statistical error).

[5] For the generation of the unweighted events $\langle w \rangle$ must be taken over all the accepted and rejected events.

is calculated by the sampler VESKO2.

For the weighted event generation the weight w is provided for each event through an appropriate event record. In the case of the unweighted event generation the rejection technique is employed. All accepted events have, therefore, the constant weight $w = 1$ and they can be viewed as the realistic physical events. The rejection rate of the algorithm is reasonably small, usually less than 20%. The example distribution of the weight $W = \kappa w$ is shown in Fig. 5. It is very regular, without $W < 0$ and $W > W_{\max}$ events, where $W_{\max} = 1.13$ is maximum weight used in the case of rejection.

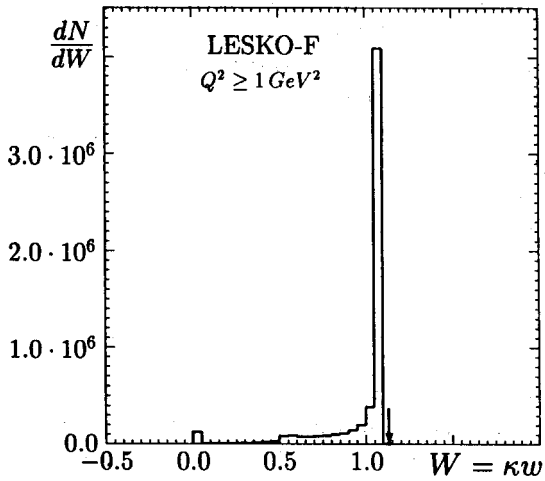

Fig. 5. The distribution of the weight $W = \kappa w$ for the example run of the program LESKO-F. The result comes from the Monte Carlo sample of $5 \cdot 10^6$ events for the KMRS-B0 parametrization [62] of the parton distribution functions. The maximum weight $W_{\max} = 1.13$, used for (eventual) rejection, is marked with the arrow. There is no events with $W < 0$ and $W > W_{\max}$.

Having the variables $t, x, z_1, z_2, \phi, \psi$ one can calculate the momenta of all particles in the final state. They are also needed to evaluate the weight w according to Eq. (47). The type of the hit quark q is picked up according to the probability

$$p_q = \frac{q_q(x,t)\rho_q(t,x,z_1,z_2,\phi,\psi)}{\varrho(t,x,z_1,z_2,\phi,\psi)}, \tag{50}$$

where ϱ and ρ_q are defined in Eqs. (22) and (29). After this generation step each event is fully characterized by the momenta and flavours of the outgoing particles, but yet at the parton level. In order to obtain the physical particles

the quark fragmentation must be performed. This problem will be discussed in Subsection 2.4.

2.2. Multiphoton leptonic radiation

In the previous subsection we have described the Monte Carlo algorithm for deep inelastic lepton proton scattering including *single QED bremsstrahlung* from the lepton line. Now we shall present the M.C. algorithm which allows for radiation of *an arbitrary number of photons.* It is based on the exclusive exponentiation procedure proposed by Yennie, Frautschi and Suura (YFS) in Ref. [31]. In brief, exponentiation is the method of summing up to infinite order the contributions from soft virtual and real photons. In Ref. [31] all the soft photon contributions/divergences are carefully analysed in the standard Feynman-diagrams based framework of QED, taking care of renormalizibility (ultraviolet divergences) and gauge invariance. This procedure represents *the exclusive exponentiation* because isolation and summation (to infinite order) of the infrared divergent contributions is done on exclusive differential cross sections (in fact on scattering amplitudes) with an arbitrary number of real and virtual photons. The remaining nondivergent parts are calculated perturbatively (order by order). For a more detailed explanation of many aspects of exponentiation we refer the reader to Ref. [63]. Monte Carlo implementation of the YFS exponentiation was started by Jadach and Ward in Refs [64] and [65], and the first M.C. program, including the YFS exponentiation, was published in Ref. [53]. The first implementation of the YFS exponentiation for a t-channel process was described in Ref. [66]. All the above prescriptions were intended for e^+e^- scattering at the LEP/SLC energies. They are, however, more general purpose in the essence and can be applied to other processes with charged particles as well, *e.g.* to deep inelastic ep scattering at HERA. The main profit of the use of the YFS exponentiation, apart from having the correct soft photons limit, is that the order by order convergence of the integrated cross sections and differential distributions is usually better than in the non-exponentiated version of calculations, see *e.g.* Ref. [67]. In the following we shall describe an implementation of the exclusive YFS exponentiation in the Monte Carlo algorithm for deep inelastic ep scattering at high energies. It is based essentially on the algorithm developed for the Bhabha scattering process at low angles, employed in the program BHLUMI [54], which includes the YFS exponentiated $\mathcal{O}(\alpha)$ QED matrix element. However, in order to adapt it to deep inelastic scattering some necessary modifications had to be made.

The complete *master formula* for the $\mathcal{O}(\alpha)$ exponentiated total cross section for the process

$$l(p_1) + p(P) \longrightarrow l(p_2) + X(P') + n\gamma(k_i) \tag{51}$$

within the framework of the QCD improved quark–parton model can be written as follows

$$\sigma = \sum_q \int_0^1 dx \sum_{n=0}^{\infty} \frac{1}{n!} \int \frac{d^3q_2}{q_2^0} \frac{d^3p_2}{p_2^0} \delta^{(4)}(p_1 + q_1 - p_2 - q_2 - \sum_{i=0}^{n} k_i)$$
$$\times e^{Y(\Omega, p_1, p_2)} \int \prod_{i=1}^{n} \frac{d^3k_i}{k_i^0} \tilde{S}(p_1, p_2, k_i)(1 - \Theta(\Omega; k_i))$$
$$\times \left(\bar{\beta}_{q,0}^{(1)}(Q, p_1, p_2, q_1, q_2) + \sum_{i=1}^{n} \frac{\bar{\beta}_{q,1}^{(1)}(Q, p_1, p_2, q_1, q_2, k_i)}{\tilde{S}(p_1, p_2, k_i)} \right)$$
$$\times q_q(x, Q^2) \Xi_{MC}(p_i, q_i, k_j), \tag{52}$$

where $q_1 = xP$ is the four-momentum of the quark in the proton to be scattered and q_2 is the four-momentum of this quark after the collision, while the non-reacting proton remnant has the four-momentum $P_X = (1-x)P$. The sum $\sum_q$ in the above formula stands for summing over all the quark flavours and $q_q(x, Q^2)$ is the quark distribution in the proton.

Other components of Eq. (52) have the following meaning:

$$\tilde{S}(p_1, p_2, k) = -\left(\frac{\alpha}{4\pi^2}\right)\left(\frac{p_1}{kp_1} - \frac{p_2}{kp_2}\right)^2 \tag{53}$$

is the real photon infrared factor, and

$$Y(\Omega, p_1, p_2) = 2\alpha \tilde{B}(\Omega, p_1, p_2) + 2\alpha \,\mathrm{Re}\, B(p_1, p_2)$$
$$= -2\alpha \frac{1}{8\pi^2} \int \frac{d^3k}{k^0} \Theta(\Omega; k) \left(\frac{p_1}{kp_1} - \frac{p_2}{kp_2}\right)^2$$
$$+ 2\alpha \,\mathrm{Re} \int \frac{d^4k}{k^2} \frac{i}{(2\pi)^3} \left(\frac{2p_1 - k}{2kp_1 - k^2} - \frac{2p_2 - k}{2kp_2 - k^2}\right)^2 \tag{54}$$

is the standard Yennie–Frautschi–Suura form factor [31]. It is infrared finite, and $\Theta(\Omega, k) = 1$ for $k \in \Omega$ and $\Theta(\Omega, k) = 0$ for $k \notin \Omega$. The infrared region Ω includes the infrared point $k = 0$ and its definition may implicitly involve the dependence on lepton four-momenta p_i. But none of the physically sensible results depend on the choice of the Ω!

The perturbative $\mathcal{O}(\alpha)$ QED matrix element is located in the $\bar{\beta}$'s which have the form:

$$\bar{\beta}_{q,0}^{(1)}(Q, p_1, p_2, q_1, q_2) = \bar{\beta}_{q,0}^{(0)}(Q, p_1, p_2, q_1, q_2)(1 + \delta_0), \tag{55}$$

$$\delta_0 = 2\,\mathrm{Re}\,F_1(Q^2) - 2\,\mathrm{Re}\,B(Q^2) = \tfrac{1}{2}\beta_t\,, \quad \beta_t = 2\frac{\alpha}{\pi}\left(\ln\frac{Q^2}{m_l^2} - 1\right), \tag{56}$$

$$\bar{\beta}^{(0)}_{q,0}(Q, p_1, p_2, q_1, q_2) = \frac{2\alpha^2}{s}\, D^{(0)}_{q,0}(Q, p_1, p_2, q_1, q_2)\,, \tag{57}$$

$$\bar{\beta}^{(1)}_{q,1}(Q, p_1, p_2, q_1, q_2) = \frac{2\alpha^2}{s}\,\frac{\alpha}{4\pi^2}\, D^{(1)}_{q,1}(Q, p_1, p_2, q_1, q_2, k_i) - \tilde{S}(p_1, p_2, k_i)\,\bar{\beta}^{(0)}_{q,0}(Q, p_1, p_2, q_1, q_2)\,, \tag{58}$$

$$t = Q^2 = (p_2 + \sum_{i=1}^{n} k_i - p_1)^2\,, \quad t_p = -2p_1p_2\,, \tag{59}$$

$$s = 2p_1q_1 = xs_0\,, \quad s_1 = 2p_2q_2\,, \quad u = -2p_1q_2\,, \quad u_1 = -2q_1p_2\,, \tag{60}$$

and $s_0 = (P + p_1)^2 \simeq 2p_1P$. The terms $D^{(0)}_{q,0}$ and $D^{(1)}_{q,1}$ are contributions to the matrix element of the lepton quark scattering subprocess including multiphoton radiation from both the initial and final lepton states. They are given explicitly in Appendix B.

The function $\Xi_{\mathrm{MC}}(p_i, q_i, k_j)$ defines the phase space for M.C. event generation. The present algorithm gives two possibilities for the phase space cut:

$$\Xi_{\mathrm{MC}}(p_i, q_i, k_j) = \Theta(p_{\mathrm{T}} - p_{\mathrm{T,min}})\,, \tag{61}$$

or

$$\tilde{\Xi}_{\mathrm{MC}}(p_i, q_i, k_j) = \Theta(\mid t \mid - \mid t \mid_{\mathrm{min}})\,, \tag{62}$$

where p_{T} is the hadronic transverse momentum, $p_{\mathrm{T}} = \sqrt{(q_2^1)^2 + (q_2^2)^2}$. As discussed in the first part of this section, the former is more realistic from the experimental point of view (it can be used as a trigger for deep inelastic events). The user's own experimental trigger Ξ_{exp} can be imitated by the rejection of some generated events.

Having defined the cross section for the process (51) we can describe the Monte Carlo algorithm for the event generation. Constructing such an algorithm consist, in general, of two steps: (1) a choice of proper integration variables and (2) simplifications of an integrand which are later compensated by appropriate rejection. To each simplification corresponds a well-defined multiplicative component in the rejection weight. The variables convenient in simulation of QED bremsstrahlung were invented during the construction of the program LESKO-F and they are described in the previous subsection, see Eq. (24) for the definition. Their generalization to the multiphoton radiation case was done in Ref. [66]. In the new variables[6] the phase space

[6] In fact, they are a generalized variant of the Sudakov light-cone variables introduced in Ref. [68].

together with the infrared singularities due to real photons appears to be treatable by the Monte Carlo methods. Following Ref. [54] we introduce them through the identity

$$\int \frac{d^3q_2}{q_2^0}\frac{d^3p_2}{p_2^0}\delta^{(4)}(p_1+q_1-p_2-q_2-\sum_{i=1}^{n}k_i) \times \int\prod_{i=1}^{n}\frac{d^3k_i}{k_i^0}\tilde{S}(p_1,p_2,k_i)(1-\Theta(\Omega_1;k)) = \int\limits_{|t|_{\min}}^{s_0}\frac{d\,|\,t\,|}{s}\int\limits_0^{2\pi}d\phi\int\prod_{i=1}^{n}d\omega_i\left|\frac{t_p}{t}\right|\Theta(s_1) \qquad (63)$$

which holds up to $m_l^2/|t|$ terms. The bremsstrahlung integration elements $d\omega_i$ can be expressed in terms of the new variables:

$$d\omega_i = \frac{\alpha}{\pi}\frac{\tilde{\alpha}_i\tilde{\beta}_i(1-\Theta(\Omega_1))d\tilde{\alpha}_i d\tilde{\beta}_i}{(\tilde{\alpha}_i+\delta_p\tilde{\beta}_i)^2(\tilde{\beta}_i+\delta_p\tilde{\alpha}_i)^2}, \quad \delta_p=\frac{m_l^2}{|\,t_p\,|}, \quad 0<\tilde{\alpha}_i,\tilde{\beta}_i<1. \qquad (64)$$

The variables $\tilde{\alpha}_i$, $\tilde{\beta}_i$ are defined in terms of the corresponding t-channel rest frame QRS_p, where $p_1^0=p_2^0=E_p$ and $\vec{p_1}+\vec{p_2}=0$, as follows

$$k_i^0=(\alpha_i+\beta_i)E_p, \quad k_i^3=(-\alpha_i+\beta_i)E_p,$$
$$k_i^1=k_T\cos\phi_i, \quad k_i^2=k_T\sin\phi_i, \quad k_T=2E_p\sqrt{\alpha_i\beta_i},$$
$$\alpha_i=\tilde{\alpha}_iK_p, \quad \beta_i=\tilde{\beta}_iK_p, \quad K_p=\left(1-\sum_{j=1}^{n}\tilde{\beta}_j\right)^{-1}=\frac{p_1p_2}{p_1(p_2+\sum_{j=1}^{n}k_j)}, \qquad (65)$$

see also Ref. [66] for more details. The condition $\Theta(s_1)$ in Eq. (63) prevents from negative values of s_1, *i.e.* outside the phase space, which may formally appear for some high values of $\tilde{\alpha}$'s and $\tilde{\beta}$'s.

After a transformation to the new variables the master formula of Eq. (52) takes the form

$$\sigma=\sum_q\int\limits_0^1 dx\sum_{n=0}^{\infty}\frac{1}{n!}\int\limits_{|t|_{\min}}^{s_0}\frac{d|t|}{s}\left|\frac{t_p}{t}\right|\int\limits_0^{2\pi}d\phi e^{Y(\Omega_1)} \times\int\prod_{i=1}^{n}d\omega_i\Theta(s_1)\bar{\beta}_q^{0+1}q_q(x,t)\Xi_{\mathrm{MC}}, \qquad (66)$$

where $\bar{\beta}_q^{0+1}$ is an abbreviation for the perturbative part of Eq. (52). The soft photon region Ω_1 and the corresponding YFS factor $Y(\Omega_1)$ is defined as in Ref. [54], *i.e.* Ω_1 is a rectangle in terms of the Sudakov-type variables,

$$\max(\tilde{\alpha}_i, \tilde{\beta}_i) < \Delta\,, \tag{67}$$

and the YFS form factor reads

$$Y(\Omega_1, p_1, p_2) = \frac{\alpha}{\pi}\left\{2\left(\ln\frac{2p_1p_2}{m_l^2} - 1\right)\ln\Delta_p + \tfrac{1}{2}\ln\frac{2p_1p_2}{m_l^2} - 1\right\}, \quad \Delta_p = K_p\Delta\,. \tag{68}$$

Having the cross section expressed in terms of the suitable variables we can use it in the M.C. generation. The variables describing the M.C. event should be generated according to the differential distribution

$$d\rho_q = \frac{1}{n!}d\phi\frac{d\,|\,t\,|}{s}\mathrm{e}^{Y(\Omega_1)}\prod_{i=1}^{n} d\omega_i\Theta(s_1)\bar{\beta}_q^{0+1}\,. \tag{69}$$

In order to do this we replace $d\rho_q$ by the appropriate "crude" density $d\rho_q^0$ which is easier for M.C. integration and generation. All effects of such a simplification are then removed by rejecting events according to the weight

$$W = \frac{d\rho_q}{d\rho_q^0}\,. \tag{70}$$

The accepted events are thus distributed according to the true density $d\rho_q$ and have the constant weight equal to one. One may, however, work with the weighted events as well. In that case rejection is not performed and each generated event is accompanied with the appropriate weight W, according to Eq. (70). In both cases the total cross section is given, up to a statistical error, by

$$\sigma = \langle W\rangle\sigma_0 = \langle W\rangle\sum_q\int_0^1 dx\sum_{n=1}^{\infty}\int d\rho_q^0 q_q(x,t)\,, \tag{71}$$

where the average weight $\langle W\rangle$ is calculated numerically and the "crude" cross section σ_0 is known semi-analytically[7].

The simplification $d\rho_q \to d\rho_q^0$ is done in the M.C. algorithm in a few steps. To each step corresponds the appropriate correction factor $W^{(k)}$ which enters the total weight W,

$$W = \prod_{k=1}^{4} W^{(k)}\,. \tag{72}$$

[7] The most complicated two-dimensional integration in σ_0 involving the proton structure functions is performed by the sampler VESKO2 [61].

In our case there are four main stages of the modification of the differential distribution:

1. First, we perform the simplification in the integration element $d\omega_i$. It is done by the following replacements

$$\delta_p \longrightarrow \frac{m_l^2}{s} = \delta_s\,, \tag{73}$$

$$\frac{\tilde{\alpha}_i\tilde{\beta}_i}{(\tilde{\alpha}_i + \delta_p\tilde{\beta}_i)(\tilde{\beta}_i + \delta_p\tilde{\alpha}_i)} \longrightarrow 1\,, \quad \left|\frac{t_p}{t}\right| \longrightarrow 1\,. \tag{74}$$

The above simplifications lead to

$$\left|\frac{t_p}{t}\right| \prod_{i=1}^{n} d\omega_i \longrightarrow \prod_{i=1}^{n} d\tilde{\omega}_i\,, \quad d\tilde{\omega}_i = \frac{\alpha}{\pi}\,\frac{\Theta(\tilde{\alpha}_i - \Delta)\Theta(\tilde{\beta}_i - \Delta)d\tilde{\alpha}_i d\tilde{\beta}_i}{(\tilde{\alpha}_i + \delta_s\tilde{\beta}_i)(\tilde{\beta}_i + \delta_s\tilde{\alpha}_i)}\,, \tag{75}$$

and the corresponding "mass weight" reads

$$W^{(1)} = \left|\frac{t_p}{t}\right| \prod_{i=1}^{n} W_i^{(1)}, \quad W_i^{(1)} = \frac{\tilde{\alpha}_i\tilde{\beta}_i(\tilde{\alpha}_i + \delta_s\tilde{\beta}_i)(\tilde{\beta}_i + \delta_s\tilde{\alpha}_i)}{(\tilde{\alpha}_i + \delta_p\tilde{\beta}_i)^2(\tilde{\beta}_i + \delta_p\tilde{\alpha}_i)^2}\,. \tag{76}$$

2. Next, in order to get rid of the complicated dependence $s_1(s,t,\tilde{\alpha}_i,\tilde{\beta}_i)$ we set

$$\Theta(s_1) \longrightarrow 1\,, \tag{77}$$

and the corresponding weight is

$$W^{(2)} = \Theta(s_1)\,. \tag{78}$$

3. For the same purpose we simplify the YFS form factor:

$$Y(\Omega_1) \longrightarrow Y_\Delta = -2\frac{\alpha}{\pi}\ln\delta_s \ln\Delta = 2\frac{\alpha}{\pi}\ln\frac{s}{m_l^2}\ln\Delta\,, \tag{79}$$

and the corresponding "form factor weight" is

$$W^{(3)} = \exp(Y(\Omega_1) - Y_\Delta)\,. \tag{80}$$

This replacement fixes, in addition, the normalization of the average total weight (in our case it is chosen such that $\langle W\rangle \simeq 1$).

4. Finally, we replace the series included in $\bar{\beta}_q^{0+1}$ by the Born-like distribution:

$$\bar{\beta}_q^{0+1} \longrightarrow b_q^0(s,t) = \frac{s}{2\pi}D_{lq}(s,t)\,, \tag{81}$$

where D_{lq} is the differential cross section for the process $lq \to lq$, given explicitly in Appendix A. For this substitution we have the important "model component weight"

$$W^{(4)} = \frac{\bar{\beta}_q^{0+1}}{b_q^0}. \tag{82}$$

The "crude" Monte Carlo cross section resulting from the above simplifications takes the form

$$\begin{aligned}\sigma_0 &= \sum_q \int_0^1 dx \sum_{n=0}^{\infty} \int d\rho_q^0 q_q(x,t)\Theta(x - x_{\min}(t)) \\ &= \sum_q \int_0^1 dx \sum_{n=0}^{\infty} \frac{1}{n!} \int_{|t|_{\min}}^{s_0} d|t| \frac{|t|}{s} \int_0^{2\pi} d\phi e^{Y_\Delta} \\ &\times \int \prod_{i=1}^{n} d\tilde{\omega}_i b_q^0(s,t) q_q(x,t)\Theta(x - x_{\min}(t)),\end{aligned} \tag{83}$$

where $x_{\min}(t) = |t|^2/s_0(|t| - p_{T,\min}^2)$. Since $\int d\tilde{\omega}_i = 2(\alpha/\pi)\ln\delta_s \ln\Delta$ we obtain the results

$$\begin{aligned}\sigma_0 &= \sum_q \int_0^1 dx \int_{|t|_{\min}}^{s_0} d|t| \frac{2\pi}{s} b_q^0(s,t) q_q(x,t)\Theta(x - x_{\min}(t)) \\ &= \int_{|t|_{\min}}^{s_0} d|t| \int_{x_{\min}(t)}^1 dx \sum_q D_{lq}(s,t) q_q(x,t),\end{aligned} \tag{84}$$

where the last two-dimensional integration is rather complicated because it involves the parton distribution functions. It is performed by the two-dimensional sampler VESKO2 [61].

Apart from the evaluation of the integrated "crude" cross section σ_0 the differential distribution $d\rho_q^0$ is used to generate randomly the phase space points $(t, x, \phi, \tilde{\alpha}_i, \tilde{\beta}_i, \phi_i)$ and the type q of the hit quark. The pair (t, x) can be generated independently of the rest of the variables which, in turn, can be generated independently of each other! The M.C. generation is performed in the following way. First, the pair (t, x) is generated with the help of the sampler VESKO2 according to the distribution

$$f(x,t) = \sum_q D_{lq}(s,t) q_q(x,t). \tag{85}$$

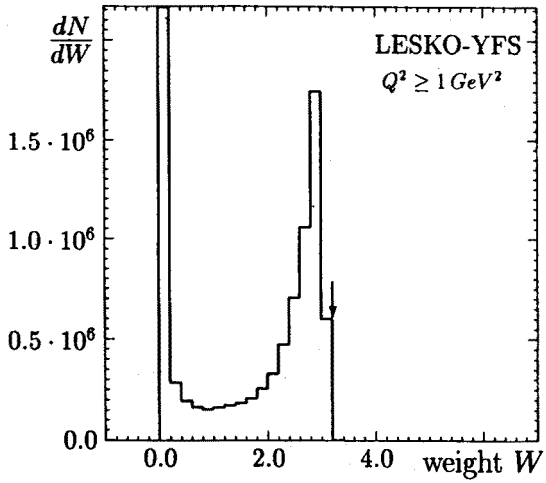

Fig. 6. The distribution of the total weight W for the multiphoton generator LESKO-YFS. The result comes from the Monte Carlo sample of $1.5 \cdot 10^7$ events for the KMRS-B0 parametrization [62] of the parton distribution functions. The maximum weight $W_{\max} = 3.06$, used for (eventual) rejection, is marked with the arrow. The events with $W > W_{\max}$, not visible in the plot, represents the fraction $(1.89 \pm 0.05) \cdot 10^{-5}$ of the total cross section. There is no events with $W < 0$. (The highest bin containing events with $W = 0$ extends to $8.7 \cdot 10^6$.)

Then the flavour q of the hit quark is picked according to the probability

$$p_q = \frac{q_q(x,t)}{f(x,t)}\,. \tag{86}$$

The other variables are generated according to their partial distributions entering $d\rho_q^0$. When all the needed variables are chosen they are subsequently translated into the final state four-momenta p_2, q_2, k_i. Then, the distributions $d\rho_q$ and $d\rho_q^0$ are evaluated for the picked out quark flavour q. In parallel to generation of the variables the component weights corresponding to each simplification step are calculated, and finally the total weight W is obtained according to Eq. (72). In order to get the variables distributed precisely according to the original distribution of Eq. (52) the rejection method, as described in the previous subsection, must be applied. An example distribution of the total weight W is shown in Fig. 6. It is regular, without $W < 0$ events and with a totally negligible tail of $W > W_{\max}$ events (their fraction of the total cross section is less than $2 \cdot 10^{-5}$), where $W_{\max} = 3.06$ is the maximum weight used in the case of rejection. In fact, the maximum weight depends on the phase space cut value $|t|_{\min}$ (or $p_{T,\min}$) — increases with decreasing $|t|_{\min}$ (or $p_{T,\min}$) — but it is automatically adjusted by the program.

The Monte Carlo algorithm described above is implemented in the program LESKO-YFS which is one of the parts of the M.C. package LESKO-E for deep inelastic electron proton scattering at HERA including QED radiative processes. Its detailed descriptions will be given elsewhere [69].

2.3. Numerical results and comments

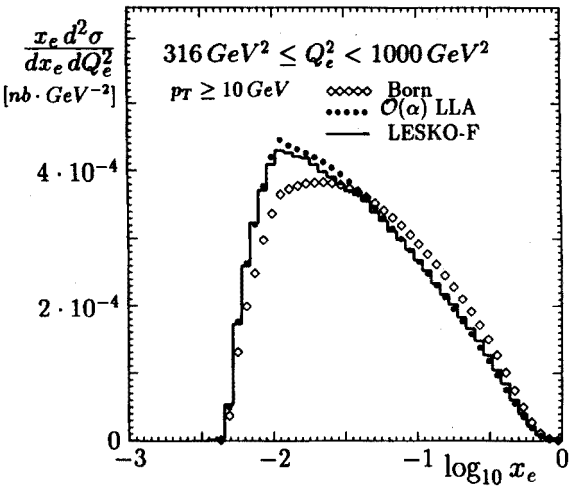

Fig. 7. Distributions of differential cross section $x_e\, d^2\sigma/dx_e\, dQ_e^2$ obtained from LESKO-F (solid line) and from analytical calculations: in the Born approximation (◇◇◇◇) and in the leading logarithmic approximation (....) for the Duke & Owens parametrization (set 1) [72] of the parton distribution functions.

After constructing a Monte Carlo events generator it should undergo a number of various tests. In particular, when a very high precision is required this ought to be done with a great care. A sort of tests the M.C. generator must undergo depends, in general, on many aspects of a simulated process. A detailed treatment of this subject is beyond the scope of this article. In a case of QED M.C. generators it is analysed *e.g.* in Refs [70, 67, 71]. Usually, the M.C. generator is checked against analytical (or semi-analytical) calculations, if possible, and/or compared with other equivalent, but independent, M.C. generators. Comparisons of existing M.C. generators and analytical programs for radiative corrections at HERA are presented in Ref. [26]. The program LESKO-F was checked in a wide kinematical range against analytical calculation in the $\mathcal{O}(\alpha)$ leading logarithmic approximation (LLA) including initial leptonic bremsstrahlung. The results for one Q_e^2-bin are shown in Fig. 7. The final state radiation in LESKO-F was treated calorimetrically, *i.e.* the four-momenta of the photons emitted close to the final

electron directions (within the angle $0.1\,rad$) were added to the electron ones ("dressed" electrons). As one could expect, the results from LESKO-F agree with the $\mathcal{O}(\alpha)$ LLA analytical calculation within the accuracy of a few per cent of the Born cross section[8]. This means that the major part of QED radiative corrections is included in the leading logarithmic terms ($\sim \ln(Q^2/m_e^2)$). From this fact one may expect that even higher order LL terms are non-negligible, especially in the regions where the first order correction are large (low x). The program LESKO-F was also compared with the event generator HERACLES based on the completely different simulation method [36]. The comparison was done for distributions of various kinematic variables in two phase space regions defined by $10^{-3} \leq x_e < 0.1$ and $0.1 \leq x_e < 0.5$. The result are presented and discussed in Ref. [26]. They show a good agreement of the both programs at the achieved statistical precision level which was determined mainly by the results of HERACLES ($\simeq 4 \cdot 10^5$ events in each of the above x_e-ranges).

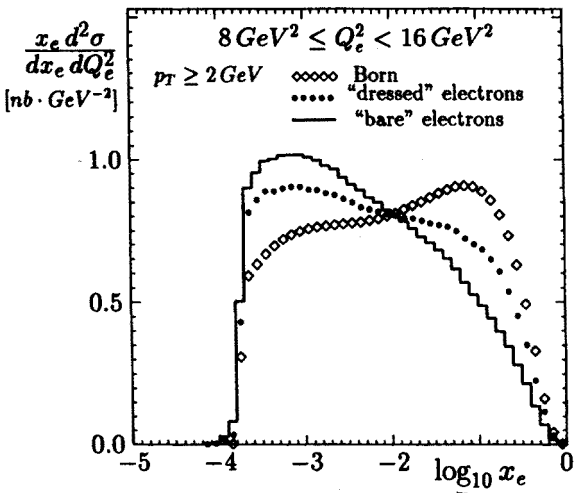

Fig. 8. Distributions of differential cross section $x_e\, d^2\sigma/dx_e\, dQ_e^2$ obtained from LESKO-F in two cases: (1) the radiative photons are not detected at all (solid line) and (2) they are detected together with the electrons when they are emitted within the angle 0.02 rad according to the electron directions (••••). They are compared with the results in the Born approximation (◇◇◇◇). All the distributions are done for the KMRS-B0 parametrization [62] of the parton distribution functions.

In Fig. 8 we show the effect of the calorimetrical treatment of final

[8] Roughly, one can expect that the subleading corrections are smaller than the leading ones by the factor $\sim \ln(Q^2/m_e^2)$, which for the considered phase space region is $\simeq 20$.

state radiation ("dressed" electrons) obtained with the help of the program LESKO-F. The final state electrons were assumed as "dressed" with the photons emitted close to their direction (within the angle 0.02 rad). Those results are compared with ones where the radiative photons are not detected at all. This analysis is done for ideal detector, no experimental effects (resolutions, misidentifications, etc.) are taken into account. From these results one can see that the calorimetrical treatment of the final state electron reduces partly the size of QED radiative corrections (final state radiation effect). This will be important for "unfolding" procedures to be discussed in the next section.

The program LESKO-YFS includes multiphoton radiation from the initial and final electron states described in the framework of the Yennie–Frautschi–Suura exclusive exponentiation including the $\mathcal{O}(\alpha)$ hard bremsstrahlung matrix element (see the previous subsection). This program was compared[9] with the program LESKO-F including single bremsstrahlung. The results for two Q_e^2-bins are presented in Fig. 9. For reference we also show the results in the Born approximation.

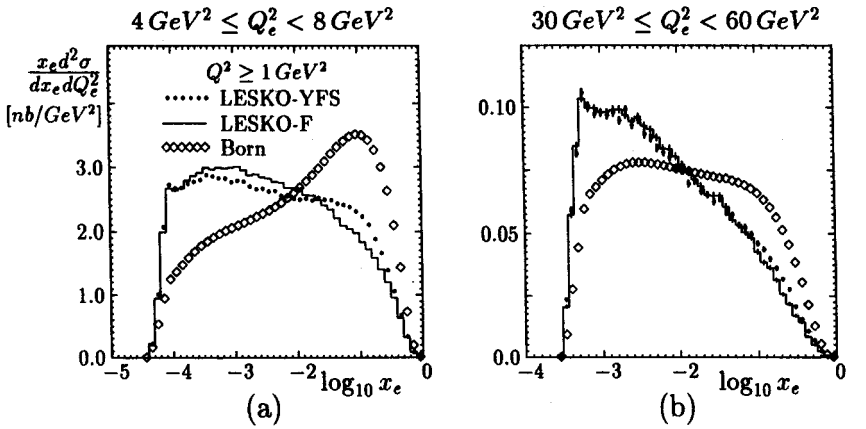

Fig. 9. Distributions of differential cross section $x_e\, d^2\sigma/dx_e\, dQ_e^2$ generated by the programs: LESKO-YFS including multiphoton leptonic radiation described by the Yennie–Frautschi–Suura type exclusive exponentiation (....) and LESKO-F including $\mathcal{O}(\alpha)$ leptonic bremsstrahlung, and obtained at the Born level (oooo). All the distributions are done for the KMRS-B0 parametrization [62] of the parton distribution functions.

One can see from Fig. 9 that higher order corrections included in the YFS

[9] The first results from LESKO-YFS were presented in Ref. [73].

exponentiation procedure give positive corrections of the size up to a few percent with respect to $\mathcal{O}(\alpha)$ distributions in the low x and high y region. The exponentiation diminish negative corrections in the range of high x and low y, *i.e.* it gives the correct soft photon behaviour. A similar effect was obtained by Bardin *et al.* in Ref. [74] as a result of including soft photon exponentiation proposed in Ref. [75]. As one can see from the comparison of Fig. 9(a) and Fig. 9(b) higher order effects decrease with increasing Q_e^2 (the distributions from LESKO-YFS get closer to ones from LESKO-F). It has been shown in Refs [51, 67] that the $\mathcal{O}(\alpha)$ YFS exclusive exponentiation includes the major part of higher order corrections. Thus, the program LESKO-YFS seems to give a sufficient QED precision for the HERA purpose.

2.4. QCD effects and hadronization

In comparison with fix target DIS experiments HERA offers a much better possibility to observe the final hadronic state. The measurements of the hadronic flow can be used to determine the phase space variables x, Q^2 and y, in some regions in parallel to the electron measurement, and even there where latter is not possible [76]. The hadronic measurement is also important from the point of view of radiative corrections unfolding. The hadronic variables are much less affected by radiative corrections than the leptonic ones, see *e.g.* Ref. [26]. This problem will be discussed in more details in the next section. The hadronic final state in DIS provides also a rich field for the study of various phenomena related to QCD [77]. Therefore, having as complete as possible description of the hadronic part is a strong desire. This problem, unfortunately, has not been ultimately solved so far. There exist several theoretical models dealing with it in different ways, see *e.g.* [77]. They are implemented in a number of Monte Carlo generators [78] which were checked against existing experimental data [79]. Most of those programs, however, do not include QED radiative corrections. On the other hand, programs for QED radiative corrections, as LESKO-F and LESKO--YFS, provide the hadronic part at the parton level only, *i.e.* in terms of the scattered quark and non-reacted proton remnant which are not the physical states. Both these programs do not include explicitly QCD radiative effects; they are included only implicitly via the scaling violating parton distribution functions. It was shown that QCD effects may significantly modify the hadronic final state at HERA [80, 79]. Because of this we have developed an interface, named FRANEQ [33], for the above QED M.C. generators and routines from the program LEPTO 5.2 treating QCD radiative effects in the framework of the parton shower (or parton cascades) picture, *i.e.* in the LLA approximation, and performing hadronization with the help the Lund string model [81] implemented in the M.C. program JETSET

6.3 [35]. The LESKO programs provide the input at the parton level to the program FRANEQ (in fact, it consist of partly modified routines from LEPTO 5.2 and some completely new ones) which subsequently generates initial and final state parton showers and turns the final partons into real physical particles. More details about dealing with QCD and hadronization one can find in Ref. [34]. The program FRANEQ is described in Ref. [33]. A similar interface for the program HERACLES [36], called DJANGO, was developed by Schuler and Spiesberger [82]. In order to have a good control of many aspects of the hadronic final state, interfaces to other M.C. programs including QCD effects and hadronization are needed[10]. This is the thing to be done in the near future.

3. Unfolding of radiative corrections

As it was pointed in the previous section a dominant contribution to the electroweak radiative corrections in deep inelastic lepton proton scattering is due to hard photon radiation from the lepton states. The size of this contribution depends on the experimental set up and the method of measuring the kinematics of the deep inelastic scattering process. In the early deep inelastic electron scattering experiments at SLAC and DESY as well as in the later muon scattering experiments at CERN and FNAL the event kinematics has always been reconstructed from the initial lepton energy, the scattered lepton energy and its angle. In the above measurement method the reconstructed leptonic (x_l, Q_l^2) can be, due to leptonic radiation, different from those characterizing the exchanged vector boson and used to specify the x and Q^2 dependence of the structure functions. As a result the differential cross section $d^2\sigma^{\text{meas}}/dx_l\,dy_l$ measured in the point (x_l, y_l) depends on the whole domain of $x \geq x_l$ and $y \leq y_l$, what symbolically can be written as follows

$$\frac{d^2\sigma^{\text{meas}}}{dx_l\,dy_l} = \int_{x_l}^{1}\int_{0}^{y_l} dx\,dy K(x_l, y_l; x, y)\frac{d^2\sigma^{\text{Born}}(x,y)}{dx\,dy}, \tag{87}$$

where the kernel $K(x_l, y_l; x, y)$ is the kinematical factor corresponding to the hard photon emission; its analytical form can be found *e.g.* in Refs [16, 18]. The integration in Eq. (87) involves the structure functions and thus the measured differential cross section for a given (x_l, y_l) depends on the shape

[10] An interface, named KROWIG, for the program KRONOS including higher order LLA QED corrections [37] and the program HERWIG [83] performing QCD effects and hadronization has recently been developed by T. Ohl [84].

of the structure functions in the wide kinematical range. The dominant contribution to the measured cross section comes from some narrow path in the kinematical domain where the kernel $K(x_l, y_l; x, y)$ is large. These paths are often called the "s-peak" and "p-peak" [14] regions because they reflect the peaking behaviour of the photon angular distribution. Other substantial contributions in Eq. (87) come from the Compton process [24] ($Q^2 \to 0$), the so called "t-peak" [14], and from elastic lepton proton scattering ($x = 1$) [27]. The last two contributions can be eliminated by restricting the Q^2 range to the DIS region, *i.e.* $Q^2 > \mathcal{O}(1)\, GeV^2$. This, however, requires additional information from the hadronic side of the process (see Section 2). A more detailed discussion of the radiative contributions to the measured cross section can be found *e.g.* in Ref. [27]. We would like only to point out that in the low x_l and high y_l range the most significant contribution comes from the s-peak region which can be identified with collinear bremsstrahlung from the initial lepton state. Radiation of hard photons almost collinear with the incoming leptons diminishes the effective beam energy and, in turn, the s-peak path is pushed towards the low Q^2 region where the differential cross section is significantly larger than at Q_l^2. Similar radiation from the final lepton state corresponds to pushing the p-peak path towards higher Q^2 where the cross section is lower than at Q_l^2, and so the contributions to the integral of Eq. (87) are much smaller than in the previous case. On the other hand, in the real experiment photons emitted almost collinear with the scattered leptons are not distinguished from the leptons. So the lepton seen in the detector is "dressed" with the photons emitted inside a cone along its direction. As was shown in the Subsection 2.4, such a treatment of the photons radiated close to the final lepton direction, so called "calorimetrical" treatment, significantly reduces corrections connected with final state bremsstrahlung. Experimental aspects of this problem are discussed in Ref. [85].

We can thus conclude from the above discussion that in DIS regime the most sizable contributions to QED radiative corrections are connected with radiation of the hard photons close to the initial lepton beam direction. In the range of small x and high y they can reach the rate of 100% or more of the Born cross section (see Subsection 2.4). Those corrections can be calculated analytically only when some shape of the structure functions is assumed in the whole kinematical domain of $x \geq x_l$ and $y \leq y_l$, where (x_l, y_l) is the point where corrections are to be evaluated. There is, however, no unique prediction for this shape from the theory so far. The structure functions are usually parametrized in terms of x for some starting value of Q^2 and then evolved to higher Q^2 by the use of the QCD evolution equations, known also as the Altarelli–Parisi equations [86]. The x-dependence of the structure functions is based on some theoretical considerations and always

involves a number of free parameters which have to be estimated from the experiment. In the region of small x the shape of the structure functions can be additionally modified by screening effects coming from recombination of partons [12]. At present there is available a large number of the structure functions parametrizations proposed by many authors. They agree in the large x domain (covered by the past experiments) but reveal big differences for small x. It was shown in Ref. [27] that also radiative corrections may differ significantly, even of the order of 30%, for various parametrizations.

All the above discussion shows that any model independent method for unfolding the Born cross section from the measured radiative cross section is strongly desired. Some kind of such a method was elaborated and employed in the classical deep inelastic experiments in SLAC. Its detailed description can be found in Ref. [14], here we only recall its essential idea trying to employ it to our formula of Eq. (87). Suppose that we want to unfold the cross section in the point (x_l, y_l). The SLAC procedure starts from the region where the nonradiative cross section is known (in Ref. [14] it is the pion threshold). Suppose that in our case it is an area of $x \geq x_0$ and $y \leq y_0$, where $x_0 > x_l$, $y_0 < y_l$. Starting from this information and using the formula (87) the nonradiative cross section is calculated for the narrow strip in the neighbourhood of the above region, and so forth until the cross section get unfolded within the entire area of $x \geq x_l$ and $y \leq y_l$. In order to do this one needs to have as many as possible experimental data points in the whole area where the cross section is to be unfolded. Apart from it some extrapolation and/or interpolation techniques have to be used to estimate the cross section in those regions of the unfolded area where the experimental data are not available (the regions between the experimental data points). This method was successfully used in the past DIS experiments, but employing it in the HERA case seems to be impossible. First of all, it is because of a wide gap between the kinematical domain covered by the previous experiments and one to be covered by HERA [76]. Furthermore, such an unfolding procedure would be difficult to control in the regions where radiative corrections are large, of order od 100%, and change rapidly. On the other hand, HERA experiments provide unique possibilities to control experimentally the size of the hard bremsstrahlung corrections. Owing to almost 4π coverage of the hadronic detection a large fraction of events containing unobserved hard initial state radiative photons can be identified on the basis of measured hadron observables. If these events are eliminated the remaining correction becomes small and, to a large extent, independent of the assumed shape of the structure functions in the unmeasured region. A sizable fraction of the hard photons radiated close to the initial electron beam can be detected in the luminosity monitor [87]. Finally, on the contrary to the past DIS experiments, the event kinematics

can be measured using the hadron detection [76] and, in this case, as was pointed out in the Subsection 1.2, leptonic hard bremsstrahlung corrections are much smaller. The measurement of the event kinematics based on the hadron detection can not be extended, however, to the large y as well as very small x [76]. In those regions the measurement of the scattered electron will remain indispensable.

At HERA, the input structure functions will have to be unfolded from the measured differential cross section by means of an iterative procedure. It is evident that the presence of radiative processes with hard unobserved photons leads to large event migrations and hence to limiting speed of an iteration convergence. In addition, a sizable part of the correction reflects the assumed shape of the structure functions in the kinematical domain, which neither has been explored by previous experiments, nor it will be measured at HERA. It is crucial therefore to provide a method of applying the radiative correction to the data in which the uncertainties due to the above effects are minimized. In the following subsections we shall present two methods for reducing radiative corrections in the data of the HERA experiments. They have been elaborated during last years, completely from the beginning, taking into account peculiarities of an electron proton collider. The first one is based on the hard radiative photon tagging with the help of the luminosity monitor. It can be used in those regions of the kinematical domain where only the electron measurement is possible, and also in the some other ones as a cross-check for other unfolding methods. In this method information from tagging events with hard radiative photons which can be detected in the luminosity monitor is used to estimate the total size of the bremsstrahlung correction. Its great advantage is that *no assumption about the shape of the structure functions is needed*! Theoretical foundations of this method are given in Ref. [39] and some experimental aspects are discussed in Ref. [40]. In the second method, described in Ref. [41], the hard initial state radiation events are tagged and rejected from the event sample on the basis of a mismatch between the observed hadronic flow and that expected from the electron measurement. The remaining corrections are small and to a large extent insensitive to the shape of the input structure functions. They may, however, be sensitive to a model dependent hadronization scheme. In this method radiative corrections are performed simultaneously with the unfolding of the experimental errors.

In the next two subsections we recall the main points of Refs [39, 40] and [41] and then give some conclusions.

3.1. Photon tagging method

A direct way of eliminating QED effects from the experimental data is to check whether a given event includes a hard photon close to the elec-

tron beam direction and to reject such an event from the sample[11]. In both HERA experiments, H1 and ZEUS, there are subdetectors monitoring photons collinear to the electron beam direction for the purpose of the luminosity measurement [88]. The polar angular coverage of those detectors is thus small, up to about 0.5 mrad with respect to the electron beam direction. Due to energy resolution limitations photons can be detected with a reliable rate only when their energy exceeds some value E_c, which for both detectors is about 3 GeV.

Let us suppose for a start that we are able to detect all the hard radiative photons carrying the energy above the fraction z_c of the electron beam energy. When we reject the events with such photons from the sample the large QED corrections due to real photon emission almost disappear. The measured cross section is still different from the Born one because of contributions from the soft and virtual photons. In the leading logarithmic approximation (LLA) and neglecting the energy loss of the electrons emitting soft photons we can derive a relation between the Born differential cross section $\sigma_B(x_e, Q_e^2)$ ($\equiv d^2\sigma_B/dx_e dQ_e^2$) and the "cut" cross section $\sigma_c(x_e, Q_e^2; z_c)$ obtained after rejecting from the data sample the tagged events with hard photons. It reads

$$\sigma_c(x_e, Q_e^2; z_c) = \left[1 + \gamma(t)\left(\ln z_0 + \frac{3}{4}\right)\right]\sigma_B(x_e, Q_e^2), \tag{88}$$

where

$$\gamma(t) = \frac{\alpha}{\pi}\ln\frac{|t|}{m_e^2}, \tag{89}$$

and

$$z_0 = \min\left\{z_c, y_e = \frac{Q_e^2}{x_e s_0}\right\}. \tag{90}$$

Equation (90) results from the observation that emission of photons having the energy fraction greater than y_e is kinematically forbidden. An estimate of the Born distribution $\sigma_B(x_e, Q_e^2)$ can be obtain from $\sigma_c(x_e, Q_e^2; z_c)$ very easily by dividing off the soft photon correction $1 + \gamma(t)(\ln z_0 + 3/4)$. The energy fraction z_c corresponding to the low photon energy cut $E_c = 3$ GeV, required by the detector, is equal to 0.1. This means that the events can be tagged only in the kinematical range of $y_e \geq 0.1$, but it is just a region where the measurement of the electron variables is possible [76].

In the real experiment radiative photons can be detected by the luminosity monitor however only within a limited polar angular range — up to

[11] In our discussion we neglect photons emitted close to the scattered electron directions assuming that in the electromagnetic calorimeter they will not be distinguished from those electrons (see the previous subsection).

$\theta_0 \simeq 0.5\,\mathrm{mrad}$ — around the electron beam direction. This means that not all events including hard radiative photons can be tagged (only a fraction of about 30%), and thus the large QED corrections can be reduced only partly. Although the "cut" cross section $\sigma_c(x_e, Q_e^2; z_c, \theta_0)$ is closer to the Born cross section $\sigma_B(x_e, Q_e^2)$ than the fully inclusive one $\sigma(x_e, Q_e^2)$, the simple formula of Eq. (88) cannot be used to obtain the estimate of the Born distribution. However, a very important observation to be noticed is that for $\theta \sim 10^{-3}$ the "cut" cross section $\sigma_c(x_e, Q_e^2; z_c, \theta_0)$ and the inclusive cross section $\sigma(x_e, Q_e^2)$ differ significantly. *The difference between these two distributions contains important information about the magnitude of QED bremsstrahlung corrections. Therefore, it is possible to obtain the estimate of the Born cross section* $\sigma_B(x_e, Q_e^2)$ *from the combined measurement of* $\sigma(x_e, Q_e^2)$ *and* $\sigma_c(x_e, Q_e^2; z_c, \theta_0)$.

As an illustration of the above remarks let us examine the dependence of QED correction on the maximal tagging angle θ. In the LLA [86] the "cut" cross section reads

$$\sigma_c(x_e, Q_e^2; z_c, \theta) = \left[1 + \gamma(t)\left(\ln z_c + \frac{3}{4}\right)\right]\sigma_B(x_e, Q_e^2) + \tilde{\gamma}(t, \theta)\int_{z_c}^{y} dz \frac{1 + (1-z)^2}{2z}\sigma_B\left(x(z), Q^2(z)\right), \quad (91)$$

where $x(z)$ and $Q^2(z)$ are easily determined by the collinear kinematics of photon emission, and

$$\tilde{\gamma}(t, \theta) = \frac{\alpha}{\pi}\ln\frac{|t|}{m_e^2 + E_b^2\theta^2} \quad (92)$$

plays the role of an effective coupling constant governing the strength of this part of QED correction which is connected with the hard photon emission (E_b is the initial electron beam energy). For perfect tagging of hard photons emitted at arbitrary angles $\tilde{\gamma} = 0$ and Eq. (91) coincides with Eq. (88), whereas for $\theta = 0$ we obtain a formula for the fully inclusive distribution $\sigma(x_e, Q_e^2)$ in the leading logarithmic approximation. For $Q^2 = |t| = 10\,\mathrm{GeV}^2$ and $\theta_0 = 10^{-3}$ the effective strength of QED bremsstrahlung, as represented by $\tilde{\gamma}(t, \theta_0)$, is reduced by about one third with respect to its maximal value for the fully inclusive case. Summarizing, we are able to manipulate (at least in principle) the strength of the initial state QED bremsstrahlung at will by changing the tagging angle. If we know the distribution $\sigma_c(x_e, Q_e^2; z_c, \theta_0)$ for two different values of θ we can eliminate the contribution of hard photon radiation in Eq. (91). In other words, we do not need to calculate the complicated integral in Eq. (91) which sums contributions from a large

region in the plane (x, Q^2) due to hard photon emission — we know it from the experiment! It is evident that we should choose $\theta = 0$, *i.e.* the fully inclusive cross section $\sigma(x_e, Q_e^2)$, and $\theta = \theta_0$, the angle which is determined by the size of the luminosity forward calorimeter. In this way we derive the following estimate of the Born cross section:

$$\sigma_{\rm B}(x_e, Q_e^2) = \frac{(1-A)\,\sigma(x_e, Q_e^2) + A\,\sigma_{\rm c}(x_e, Q_e^2; z_c, \theta_0)}{1 + \gamma(t)\left(\ln z_0 + \frac{3}{4}\right)}, \tag{93}$$

where

$$A = \frac{\ln \frac{Q^2}{m_e^2}}{\ln \frac{E_b^2\,\theta_0^2}{m_e^2}}, \tag{94}$$

and z_0 has been defined in Eq. (90). Apart from its simplicity, the most important advantage of the above formula is that all the distributions are taken at the same point (x_e, Q_e^2). There is no need to unfold the structure functions from integral equations.

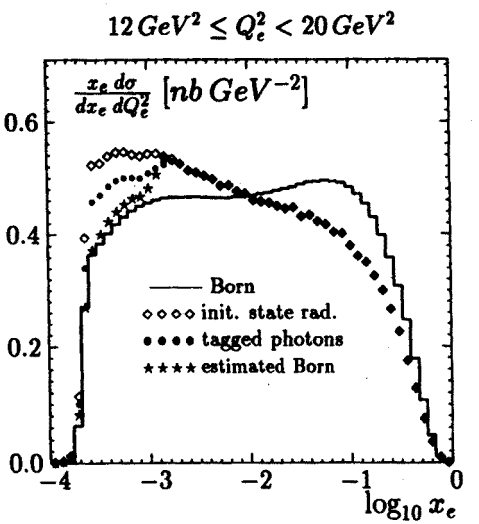

Fig. 10. The distributions of the Born cross section $\sigma_{\rm B}(x_e, Q_e^2)$ (solid line), the fully inclusive cross section $\sigma(x_e, Q_e^2)$ (◇◇◇◇), the "cut" cross section $\sigma_c(x_e, Q_e^2; z_c, \Theta_0)$ (••••) for $\Theta_0 = 5 \cdot 10^{-4}$ rad and $E_c = 3$ GeV, and the estimate of the Born cross section (★★★★) obtained from Eq. (93) for $12\,\mathrm{GeV}^2 \le Q_e^2 < 20\,\mathrm{GeV}^2$ and the hadronic $p_{\rm T} \ge 2$ GeV in a case of the precise hard photon trigger $E_\gamma \ge E_c = 3.0$ GeV. The results are given for the KMRS-B0 parametrization of the parton distribution functions [62].

In order to check the efficiency of the presented unfolding method, and in particular the accuracy of Eq. (93), we performed a Monte Carlo study. A large event sample (about $4 \cdot 10^6$ events) was generated with the help of the M.C. program LESKO-F [29] including $\mathcal{O}(\alpha)$ QED bremsstrahlung from the initial and final electron states. The events were generated with basic requirement that hadronic $p_T \geq 2\,\mathrm{GeV}$ which corresponds roughly to $Q^2 > p_T^2 = 4\,GeV^2$. Photons emitted within 0.05 rad cone around the directions of the scattered electrons were treated in the calorimetrical-like way, *i.e.* their four-momenta were added to the four-momenta of the corresponding electrons. In this study we used the parton distribution functions in the KMRS-B0 parametrization [62]. An example of the results we have obtained is presented in Fig. 10. It shows four differential distributions versus x_e for one range in Q_e^2: $12\,\mathrm{GeV}^2 \leq Q_e^2 < 20\,\mathrm{GeV}^2$. The fully inclusive cross section $\sigma(x_e, Q_e^2)$ is denoted by diamonds while the "cut" cross section $\sigma_c(x_e, Q_e^2; z_c, \theta_0)$, obtained after rejection of the tagged events with hard collinear photons, by full circles. As one can see, the both distributions agree in the region where emission of hard photons with the energy above $E_c = 3\,\mathrm{GeV}$ is kinematically forbidden, for $y_e < z_c$ ($z_c = 0.1$ in our case). Differences between them appear, however, when y_e exceeds the value z_c (it corresponds to the low x_e region in Fig. 10) and the hard photon emission becomes allowed. They are significant and rise with increasing y_e. The "cut" cross section, although closer than the fully inclusive one, is still far from the exact Born cross section (solid line in the picture). However, when we use the formula of Eq. (93) utilizing the both measured distribution, we obtain the result (stars in Fig. 10) which is very close to the Born distribution. The remaining correction are small, of order of a few per cent, whereas the original one are of order of a few dozens per cent. Estimation of the nonradiative cross section is better for higher y_e where more hard photons are emitted and hence radiative correction are bigger.

In the above discussion we have not taken into account the experimental effects of the photon tagging in the real luminosity monitor, as a finite resolution of the photon energy measurement and contaminations from other QED radiative processes. Let us first discuss the problem of photon energy measurement in the detector which is needed to answer the question whether or not in a given deep inelastic collision there was radiated photon with the energy at least E_c. In the electromagnetic calorimeter the energy of photons can be measured only with some finite resolution $\sim \sqrt{E_\gamma/\mathrm{GeV}}$. In the real experiment this measurement is additionally spoiled by a carbon filter which is placed on the way of the photon passage before the calorimeter in order to absorb the soft synchrotron radiation photons. Hard radiative photons passing through such an absorber can lose part of their energy. As a result the energy measured in the detector can differ even significantly from the

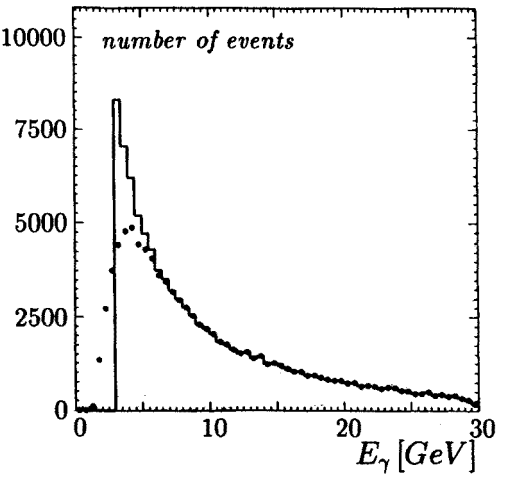

Fig. 11. The energy distributions of tagged photons in two cases: 1) for the precise hard photon trigger $E_\gamma \geq E_c = 3\,\mathrm{GeV}$ (solid line), and 2) for the lower cut $\langle E_{\mathrm{meas}}(E_c)\rangle$ imposed on the energy deposit in the luminosity calorimeter (...).

energy of the emitted photon. Therefore, we are not able to introduce the precise trigger $E_c = 3\,\mathrm{GeV}$ for emitted photons, we can only impose some lower cut on the energy deposit in the calorimeter after the filter. This cut should be chosen such that it approximates the desired trigger $E_\gamma \geq 3\,\mathrm{GeV}$ as good as possible. With the help of the Monte Carlo model of the luminosity monitor [89] we found such cuts for three values of the filter thickness: $2.5X_0$, $3.0X_0$ and $3.5X_0$ (X_0 – the radiation length), and then we used them in the M.C. simulation of hard photon tagging. Fig. 11 presents the distribution of tagged hard photons in the luminosity counter obtained for the trigger $E_{\mathrm{meas}} \geq \langle E_{\mathrm{meas}}(E_c)\rangle$ corresponding to the filter thickness $3X_0$ (full circles). For a comparison there is also shown the distribution of emitted photons with the energy above $E_c = 3\,\mathrm{GeV}$ hitting the luminosity detector window. Because of nonprecise energy measurement some photons with the energy below E_c are tagged whereas some others with the energy above E_c remain untagged.

The next experimental effect which may significantly influence the presented photon tagging method is a radiation background coming from other than DIS processes. In high energy electron proton beam collisions the main source of hard photons which can be detected in the luminosity monitor is the radiative elastic scattering process $ep \to ep + \gamma$. The cross section for the above process is much higher than for the corresponding deep inelastic process. Photons emitted in the elastic scattering process are almost collinear to the initial electron beam direction (almost 100% within the

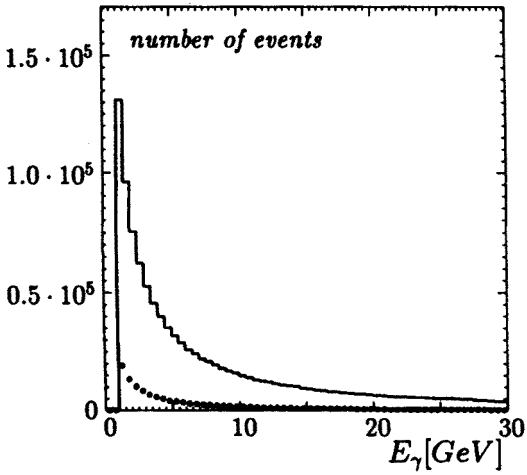

Fig. 12. Photon energy spectra observed in the luminosity monitor in coincidence with deep inelastic scattering events of $p_T^{had} \geq 2\,\mathrm{GeV}$: (1) without a background (deep inelastic radiation only — (....)) and (2) when the elastic radiation background is added (solid line). (Note: A perfect energy resolution of the detector is assumed for this plot.)

luminosity detector angular range). Part of them, with the energy above 9 GeV, will be used for the purpose of the luminosity measurement. Such photons can be well identified as coming from the radiative elastic scattering process because corresponding to them electrons can also be detected in the luminosity counter [88, 87]. The problem is, however, with photons carrying energy below $\simeq$ 9 GeV which cannot be identified on the base of the electron energy measurement. Because of random coincidences with deep inelastic events they can mimic photons coming from the radiative DIS process and/or give additional energy deposit in the detector. Fig. 12 shows photon energy spectra observed in the luminosity monitor without the elastic radiation background (deep inelastic process only — full circles) and when the background photons are added (solid line).

One can see that due to the background the luminosity monitor detects much more photons than are emitted in the DIS process and, as a result, too many deep inelastic events will be tagged. Is there any way to eliminate so high background from the data? In our opinion — YES! We have found such a way and tested it in the M.C. simulation. It is based on a simple observation that in the DIS process radiation of photons carrying the energy fraction z_c of the initial electron beam is *kinematically forbidden* in the range of $y_e < z_c$. Therefore, as can be seen in Fig. 10, the "cut" cross section, obtained after tagging and rejecting hard photon events, should agree with

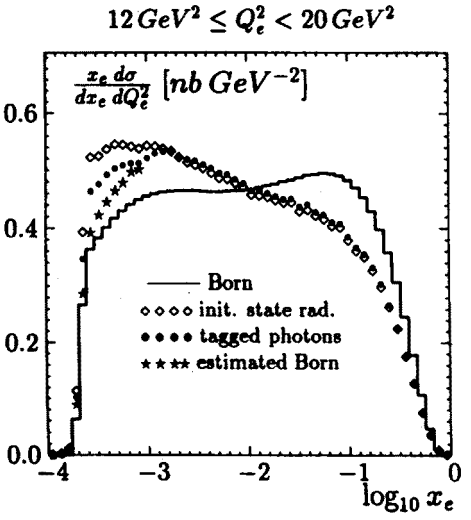

Fig. 13. The distributions of the Born cross section $\sigma_B(x_e, Q_e^2)$ (solid line), the fully inclusive cross section $\sigma(x_e, Q_e^2)$ (◇◇◇◇), the "cut" cross section $\sigma_c(x_e, Q_e^2; z_c, \Theta_0)$ (••••) for $\Theta_0 = 5 \cdot 10^{-4}$ rad, and the estimate of the Born cross section (⋆⋆⋆⋆) obtained from Eq. (93) for $12\,\mathrm{GeV}^2 \le Q_e^2 < 20\,\mathrm{GeV}^2$ and the hadronic $p_T \ge 2\,\mathrm{GeV}$ in the case when the experimental effects due to non-precise photon energy measurement in the luminosity monitor (in the presence of the $3.0\,X_0$ thick carbon filter) and the elastic scattering radiation background ($0.5 - 9.0\,\mathrm{GeV}$) are included. The background effects are eliminated from the data by adjusting the "cut" cross section to the fully inclusive one in the point $y_e = z_c = 0.1$. The results are given for the KMRS-B0 parametrization of the parton distribution functions [62].

the fully inclusive one in the above kinematical region. Any differences between them in that area are the result of the background influence. We can thus normalize the whole "cut" cross section distribution such that at the line $y_e = z_c$ (or any line $y_e = z$, $z < z_c$) it agrees with the fully inclusive distribution. Results of such a treatment are shown in Fig. 13 for one Q_e^2 bin; results for other bins are similar. They include also effects of the finite experimental resolution of the photon energy measurement in the calorimeter accompanied with the carbon absorber. The estimate of the Born cross section from the photon tagging in this case is also much closer to the original one that both the fully inclusive and "cut" distributions, however the remaining corrections are larger than ones in Fig. 10. They includes part of the background which cannot be eliminate in the described way. More details about the experimental aspects of the photon tagging method can be found in Ref. [40].

Let us discuss possible improvements of the presented method. The basic formula (93) for estimating the Born cross section is derived in the $\mathcal{O}(\alpha)$

leading logarithmic approximation. One might try to obtain a similar formula taking into account the whole $\mathcal{O}(\alpha)$ QED calculation. This, however, cannot be achieved without integration involving the structure function. In the contrary to Eq. (93), such a formula could not be applied directly to the data, but it would require some assumptions about the shape of the structure functions in the unmeasured area. A better way to improve the physical accuracy of Eq. (93) seems to be inclusion of the $\mathcal{O}(\alpha^2)$ leading logarithmic corrections and/or the soft photon exponentiation which, as discussed in Section 2, is the most effective way of including higher order corrections. The main uncertainty in this method is, however, of the experimental origin. First of all, it can be apparently reduced if the identification of the background photons in the luminosity monitor system is extended to energies from about 1 GeV up to 30 GeV. The accuracy of the method could also be improved, particularly at lower y (in our case near the value 0.1) when the photon energy measurement in the luminosity detector is extended to lower values of the photon energy (less than 3 GeV). In such a situation the soft photon approximation of Eq. (91) would provide a smaller uncertainty than in the discussed case, where it corresponds to the photon energy cut $E_c = 3$ GeV.

We can conclude the above discussion that the proposed method of reducing QED radiative correction in deep inelastic electron proton scattering by hard photon tagging in the luminosity monitor can be applied in the HERA experiments, as well as in the eventual future experiments at LEP/LHC, especially in the region of small x and high y where radiative corrections are the biggest.

3.2. Combined electron and hadron measurement

The method presented below exploits simultaneous measurement of the scattered electron energy, its angle and the longitudinal hadronic energy flow in order to reconstruct the missing longitudinal energy of the projectile electron. The reconstructed missing energy can then be used to tag hard photon initial state radiation events. If these events are rejected, the remaining radiative correction becomes small, almost insensitive to the assumed shape of the structure functions in the unmeasured region, and large event migrations are avoided. A toy model of the apparatus has been used to study the detector smearing and acceptance correction folded with the radiative correction. It has to be stressed that the efficiency of radiative event tagging is almost uniquely determined by the detector ability to measure the energy and the angle of hadrons in the wide angular range.

The emission of photons in a direction close to the incident electron can be interpreted as a reduction of the effective electron beam energy. The effective electron energy E_{eff} (or the missing energy $E_{\text{mis}} = E_o - E_{\text{eff}}$),

where E_o is the nominal energy of the electron beam, can be calculated from the scattered electron energy E_e, the angle θ_e and from the hadronic momenta p_h and the angles θ_h ($+z$ axis of the laboratory frame assumed along the proton beam), in the following way:

$$E_{\rm mis} = E_o \frac{y_e - y_t}{1 - y_t}, \tag{95}$$

where

$$y_e = 1 - \frac{E_e}{E_o} \sin^2 \frac{\theta_e}{2}, \quad y_t = \frac{1}{1 + \frac{E_e}{u} \sin^2 \frac{\theta_e}{2}}, \tag{96}$$

and

$$u = \tfrac{1}{2} \Sigma_h (E_h - p_h \cos\theta_h). \tag{97}$$

Note, that the $E_{\rm mis}$ can be equivalently expressed by the y_e and $y_{\rm JB}$ (the Jaquet–Blondel variables [90]) as

$$E_{\rm mis} = E_o (y_e - y_{\rm JB}). \tag{98}$$

For the Born events one expects $E_{\rm mis} = 0$, whereas for the radiative events with hard unobserved photons emitted collinearly with the incoming electron $E_{\rm mis}$ is equivalent to the sum of the energy E_γ of these photons. For the finite $p_{\rm T}$ photon emission the condition $E_{\rm mis} = E_\gamma$ is fulfilled approximately as the emission angle is small (of the order of $\sqrt{m_e/E_o}$).

Once the effective electron energy is known, each deep inelastic scattering event can be characterized by the initial state radiation independent variables

$$\begin{aligned} x_t &= \frac{(E_o - E_\gamma) E_e \cos^2 \frac{\theta_e}{2}}{E_P (E_o - E_\gamma - E_e \sin^2 \frac{\theta_e}{2})}, \\ y_t &= 1 - \frac{E_e}{E_o - E_\gamma} \sin^2 \frac{\theta_e}{2}, \\ Q_t^2 &= 4 E_e (E_o - E_\gamma) \cos^2 \frac{\theta_e}{2}. \end{aligned} \tag{99}$$

With E_P we denoted the energy of the proton beam. The later variables have to be used to describe the interaction of the virtual photon with the hadronic system and they enter as arguments in the structure functions. If one defines z as

$$z = \frac{E_o - E_\gamma}{E_o}, \tag{100}$$

one can write simple relations between the above variables and the corresponding variables determined from the electron energy and angle

$$Q_t^2 = z Q_e^2, \quad x_t = \frac{x_e y_e z}{y_e + z - 1}, \quad y_t = \frac{y_e + z - 1}{z}. \tag{101}$$

Using both sets of variables, the initial state radiative events can be tagged as those where a significant difference between the reconstructed x_e, y_e, Q_e^2 and the corresponding x_t, y_t, Q_t^2 is observed.

In order to find out to which extent the radiative corrections can be reduced by applying the presented above reconstruction method with the radiative events tagging, we performed a Monte Carlo study with the help of the event generator FRANEQ [33]. This generator provides the Born as well as radiative events with real photons in the final state. The hadronization of the quark final state is performed within the Lund model using the JETSET 6.3 routines [35] and QCD radiative corrections are described in the framework of the parton shower picture. A sample of events corresponding to the integrated luminosity of 40pb^{-1} has been generated. We have decided to consider 64 bins which cover in the x range from 10^{-4} up to 10^{-2} and in the y range from 0.1 up to 0.9. Both in x and y the bin sizes are greater than 2σ of the detector resolution. Thus, migration of events from one bin into another due to apparatus effects should be small. In order to increase the efficiency of the generation we required the p_T of the hadronic system to be larger than 2 GeV. The x and y can be either x_e and y_e or x_t and y_t depending on the reconstruction scheme applied. If the electronic ones are used, then the p_T cut rejects a small fraction of hard photon radiation events, which have migrated from the low Q_t^2 region to the bins considered in this analysis. In order to control this contribution we have used the HERACLES event generator [36], in which events are generated in the electronic variables. Two sets of the parton distribution functions: the MT-S set [91] and the HMRS-E set [92] have been used in the event generation programs.

In a real experiment, the reconstructed energy E_γ will be distributed around its true value but with large tails extending to large E_γ values. This is due to experimental errors in the measurements of energies and angles, and due to the beam hole in the direction of projectile electron. As this effect can mimic an initial state radiation process it has to be studied simultaneously. In order to perform such a study we have smeared the kinematic variables according to a toy model of the detector in which hadron energies are measured with the resolution od $0.55\sqrt{E}$, the electron energy is measured with the resolution of $0.15\sqrt{E}$, the angle of particles is measured with the resolution of 10 mrad up to the angle of 175 deg (with respect to the proton beam). For each generated and smeared event the electronic variables x_e, Q_e^2, y_e, the "true" variables x_t, Q_t^2, y_t, and the E_γ were reconstructed. The energy of all radiative photons emitted in a cone of 100 mrad along the scattered electron direction was added to the scattered electron energy prior to the event reconstruction. Then, the differential cross sections $(d\sigma_{\text{Bor}}^{\text{gen}}/dxdy)$ for the generated Born events, $(d\sigma_{\text{rad}}^{\text{gen}}/dxdy)$ for the

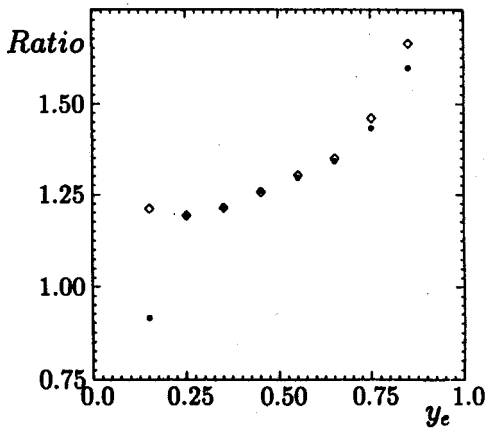

Fig. 14. The radiative correction $(d\sigma^{\rm gen}_{\rm rad}/dxdy)/(d\sigma^{\rm gen}_{\rm Bor}/dxdy)$ (••••) and the total acceptance correction $(d\sigma^{\rm obs}_{\rm rad}/dxdy)/(d\sigma^{\rm gen}_{\rm Bor}/dxdy)$ (••••) as a function of y_e for $4 \cdot 10^{-4} \leq x_e \leq 8 \cdot 10^{-4}$.

generated radiative events, $(d\sigma^{\rm obs}_{\rm Bor}/dxdy)$ for the smeared and accepted Born events and $(d\sigma^{\rm obs}_{\rm rad}/dxdy)$ for the smeared and accepted radiative events were calculated in each x_e, y_e bin.

In Fig. 14 we show the comparison of the radiative correction factors $(d\sigma^{\rm gen}_{\rm rad}/dxdy)/(d\sigma^{\rm gen}_{\rm Bor}/dxdy)$ and the total acceptance correction factors $(d\sigma^{\rm obs}_{\rm rad}/dxdy)/(d\sigma^{\rm gen}_{\rm Bor}/dxdy)$ plotted versus y_e for one of the x_e bins. The x_e, y_e dependent total acceptance correction factors include both the effect of radiation and the effect of the detector smearing. In a method of simultaneous unfolding detector and radiative effects, the measured cross section values in each bin have to be divided by these factors in order to determine the Born cross section values. It is clear, that the total acceptance correction is large and dominated by the radiative correction, the effect of the detector smearing being visible only in the large y_e region.

In Fig. 15 the generated and reconstructed spectrum of radiative photons are shown for a (x_e, y_e) bin. The peak at $E_\gamma = 0$ corresponds to the Born contribution (including final state radiation events with photons collinear to the outgoing electron), whereas the peak at $E_\gamma = y_e E_o$ corresponds to the low Q_i^2 hard initial state photon bremsstrahlung events. The events between these peaks are coming from two sources: from the initial state medium energy photon emission, and from these out of the Born events in which high momentum hadron (hadrons) were emitted in the direction of the beam hole in the electron hemisphere.

On the basis of the above plot we can now tag the hard radiation events and reject them from the event sample. A value of $E_{\rm cut}$ above which all events are classified as "hard initial photon events" has to be suitably cho-

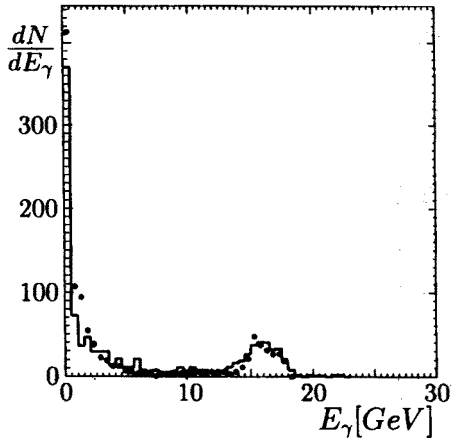

Fig. 15. The generated (solid line) and the reconstructed (....) spectrum of the energy of radiative photons for $4 \cdot 10^{-4} \leq x_e \leq 8 \cdot 10^{-4}$ and $0.5 \leq y_e \leq 0.6$.

sen and is different for detectors having different angular coverage of hadron energy measurement (the E_{cut} value chosen for the (x_e, y_e) bin shown in Fig. 15. was 6.5 GeV). If too low value is chosen the Born events are often classified as radiative. In this case the radiative correction is significantly reduced, at the expense of a systematic uncertainty in the E_γ-tails estimation. In this estimation one has to rely on a fragmentation model in order to evaluate the energy of hadrons emitted into the beam hole. If, on the other hand, too high value is used the uncertainty due to hadronization is avoided, but the radiative corrections remain large. The detailed discussion of systematic uncertainties in the total acceptance correction as a function of the E_γ cut chosen, is beyond the scope of this note and will be reported elsewhere [93].

One can also identify and reject hard initial state radiation events on the basis of the differences between the reconstructed ("true") and electronic x, y and Q^2. We have found that the efficiency of radiative events tagging using these variables is similar to the one based on the reconstructed energy E_γ.

The effect of a reduction of the total acceptance correction owing to tagging and rejecting hard initial state bremsstrahlung events is shown in Fig. 16. The acceptance correction becomes small and independent of y_e. Similar effect is observed in the other x bins. In addition, as it is shown in Fig. 17, the total acceptance correction becomes independent of the shape of the structure functions used in the generation of the deep inelastic event sample.

Finally, it has to be stressed that by tagging and rejecting hard initial state radiation events one becomes insensitive to an assumption of the structure functions shape in the low-Q_t^2 region. This is illustrated in Fig. 18

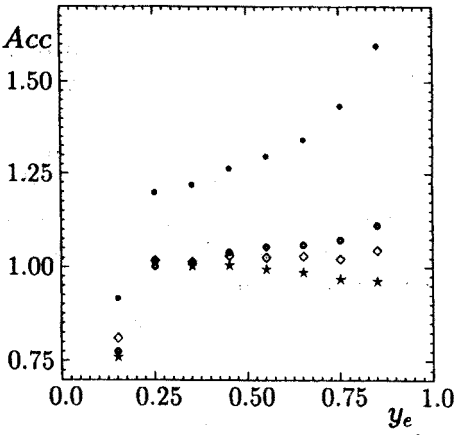

Fig. 16. The total acceptance correction $(d\sigma^{\rm obs}_{\rm rad}/dxdy)/(d\sigma^{\rm gen}_{\rm Bor}/dxdy)$ for $4\cdot 10^{-4} \leq x_e \leq 8\cdot 10^{-4}$ plotted versus y_e: no cut on hard radiation events (••••), E_γ cut applied (····), $\frac{y_e-y_t}{y_t}$ cut applied (∘∘∘∘), $\frac{Q_e^2-Q_t^2}{Q_t^2}$ cut applied (∘∘∘∘).

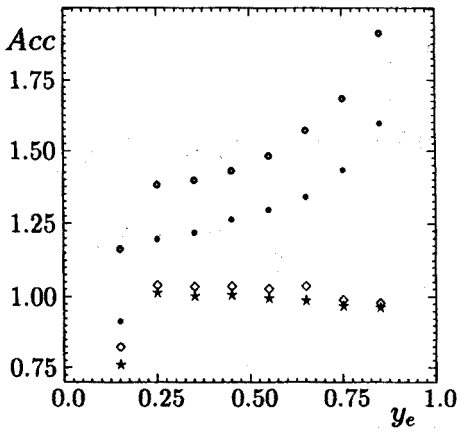

Fig. 17. The quark distribution parametrization dependence on the total acceptance correction $(d\sigma^{\rm obs}_{\rm rad}/dxdy)/(d\sigma^{\rm gen}_{\rm Bor}/dxdy)$: HMRS-E set of parton distributions, no hard photon tagging (∘∘∘∘), MT-S set of parton distributions, no hard photon tagging (••••), HMRS-E set of parton distributions, hard photon tagging (∘∘∘∘), MT-S set of parton distributions, hard photon tagging (····).

where the ratio of the differential cross sections for events restricted by the condition $Q_t^2 \geq 4\text{GeV}$, to the fully inclusive sample (no restriction on the Q_t^2 value) is shown as a function of y_e at a fixed x_e. If hard initial state radiation events are not rejected, the contribution of low Q_t^2 events may be

as large as 20 % in the large y_e region.

We have demonstrated that the identification of hard initial state radiative events is feasible at HERA. If these events are rejected from the bulk of observed events the radiative corrections are drastically reduced, and become almost insensitive to the shape of the input structure functions. It has to be mentioned, however, that the above method may be sensitive to the model dependent hadronization. In addition it requires a fairly good understanding of the resolution tails of the longitudinal hadronic energy flow measurement. The method presented here should then be considered as complementary to the method based on fully inclusive electron measurement.

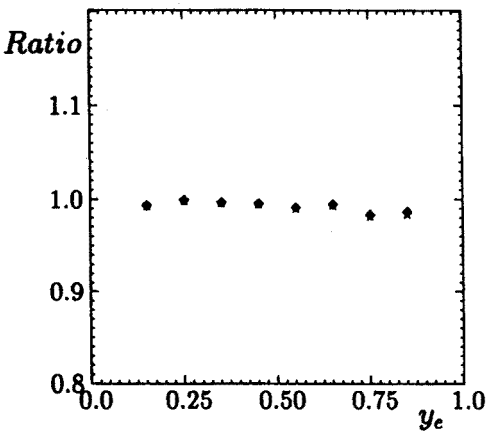

Fig. 18. A fraction of observed events in the x_e, y_e bins which migrated from the region of $Q_t^2 < 4\text{GeV}$ — $(d\sigma_{\text{rad}}^{\text{obs}}/dxdy)(Q_t^2 \geq 4)/(d\sigma_{\text{rad}}^{\text{obs}}/dxdy)(all)$.

3.3. Concluding remarks

In the above two subsection we have discussed two methods for reducing QED radiative corrections at HERA.

- The first one is based on the final electron momenta measurement and tagging events including hard radiative photons with the help of the luminosity monitor system. In this method the size of QED radiative corrections is determined directly from the data, no assumption about the shape of the structure functions is needed. It can be applied in the phase space area of $y > 0.1$ and it is especially suited for those regions where the hadron measurement is limited [76]. The main uncertainty of this method results from the subtraction of the radiative elastic scattering background. We have proposed to reduce the background effects by

normalizing the tagged events at low y where no hard radiative photons from the deep inelastic process are expected. Further improvement can be achieved only if the identification of radiative elastic scattering photons in the luminosity monitor system is extended to lower energies, of about 1 GeV. The accuracy of estimating the nonradiative cross section can also be improved, especially at lower y's (in our case for y near 0.1), if the lower cut E_c of the photon energy measurement in the luminosity detector is lowered.

- In the second method presented in Subsection 3.2 radiative corrections are treated simultaneously with the unfolding of experimental errors. The radiative events with the hard photon emitted by the incoming electron are identified and rejected from the event sample by means of measuring the hadronic energy flow associated with the scattered electron. When such events are rejected from the sample the remaining corrections become small and to the large extent insensitive to the assumed shape of the structure functions. The efficiency of this method depends crucially on the angular range in which the hadron energy measurement can be performed. It may also be sensitive to the used hadronization scheme. As there is not a unique model to describe the hadronization process at HERA, this method should be tested for various hadronization schemes.

It is evident that the above methods have different sources of the systematic errors. Therefore, it would be good if each of them is applied to the data. They can be used to make the first estimate of the nonradiative cross section at HERA. In order to unfold the structure functions from the measured differential cross section, a self-consistent iterative procedure will have to be applied. The estimates given by the presented methods can be used as good starting distributions for the unfolding iterations. The iterative procedure should be stable numerically as well as quickly convergent because the remaining corrections of the starting distributions will be small.

In Ref. [94] the authors describe an iterative method of determining the Born cross section from the fully inclusive radiative cross section when only the scattered electron is measured. In this method, which has already been applied to the data of several fixed target deep inelastic experiment, radiative corrections are estimated and then subtracted in a way of subsequent iteration steps, where as a starting distribution the radiative cross section is used; for details see Ref. [94]. It has been shown that the iteration converges if the measurement of the radiative cross section is made over all the kinematical domain. This is, however, not the case at HERA where a wide range of the x_e, Q_e^2 plane will remain unexplored [76]. The uncertainty inherent to this method is thus proportional to the contribution to the radiative cross section coming from the unmeasured region. As was

shown in Ref. [27], this contribution can be large, and thus the unfolded Born cross section can be significantly distorted if a wrong choice of the input structure functions is made.

4. Determination of the longitudinal structure function from radiative events

In the early deep inelastic experiments, the measurement of the longitudinal structure function established the fact that the charged constituents of a nucleon carry spin one half. HERA provides a unique opportunity of extending this measurement down to the low-x region of $x \simeq 10^{-4}$ where new phenomena may appear [12, 13]. In QCD, the presence of gluons interacting with quarks leads, predominantly in the low-x region, to a sizable value of the longitudinal structure function [62]. Its measurement can thus serve to constraining the gluon distribution function, as was discussed in Ref. [46].

In order to separate $F_{\mathrm{L}}(x, Q^2)$ from $F_2(x, Q^2)$ in the cross section for $ep \to eX$, it is necessary to measure the variation of the cross section with the center-of-mass energy. Emission of photons in a direction close to the incident electrons can be interpreted as a reduction of the effective electron beam energy. This effective beam energy can be determined from the energy of hard photons observed with the help of the luminosity monitor of H1 or ZEUS [88]. From the study of radiative corrections to deep-inelastic electron proton scattering at HERA it is known that especially at small x the cross section for radiative scattering is large and can reach the order of magnitude of the lowest order non-radiative cross section. We therefore propose to use the process

$$e + p \to e + \gamma + X \tag{102}$$

with a hard photon in the electron direction as a means to study the longitudinal structure function at HERA.

We will show below that the spectrum of bremsstrahlung photons in the electron direction is sufficiently hard, so that enough statistics can be reached also for small effective beam energies. Moreover, we will present results of a detailed investigation of some experimental problems to be faced at in the real measurement. We find that corrections due to a cut in the transverse momentum and bin size corrections can be quite large for small Q^2 and large photon energies. However, these corrections are determined by the $1/Q^4$ falloff of the cross section and depend very little on the structure function input. Therefore they can be reliably estimated. We also studied systematic effects coming from the reconstruction of the photon energy in the forward calorimeter and from the photon background of Bethe-Heitler quasi-elastic electron proton scattering $ep \to ep\gamma$. It was shown that these

latter effects do not introduce systematic uncertainties which exceed the statistical accuracy. More detailed discussion of the experimental aspects of the presented method can be found in Ref. [42].

4.1. "Radiative" reduction of the beam energy

We start with a discussion of the cross section for the emission of hard photons. Since we are interested in events where the polar angle θ_γ of the bremsstrahlung photon (measured with respect to the proton beam) is close to π, $\pi - \theta_\gamma < 1$ mrad, it is justified to use the collinear approximation in the following discussion. We use the common kinematic variables

$$Q_e^2 = -(p_e - p'_e)^2\,, \quad x_e = \frac{Q_e^2}{2P(p_e - p'_e)}\,, \quad y_e = \frac{P(p_e - p'_e)}{Pp_e}\,, \quad Q_e^2 = x_e y_e S\,. \tag{103}$$

Here, p_e (p'_e) and P denote the 4-momenta of the incoming (scattered) electron and of the proton and $S = (p_e + P)^2$. Emission of a photon with 4-momentum k leads to a shift of these variables to

$$Q^2 = -(p_e - p'_e - k)^2\,, \quad x = \frac{Q^2}{2P(p_e - p'_e - k)}\,, \quad y = \frac{P(p_e - p'_e - k)}{P(p_e - k)}\,. \tag{104}$$

These latter variables have to be used to describe the interaction with the hadronic system and enter as arguments in the structure functions. The definition of y in Eq. (104) is appropriate for the description of initial state radiation. In this case, *i.e.* for collinear photons $\vec{k} \parallel \vec{p}_e$ it is also suitable to parametrize the photon energy E_γ with the help of

$$z = \frac{E_e - E_\gamma}{E_e}\,, \tag{105}$$

where E_e is the energy of the incoming electron. Using this definition, one can rewrite Eq. (104) as

$$Q^2 = zQ_e^2\,, \quad x = \frac{x_e y_e z}{y_e + z - 1}\,, \quad y = \frac{y_e + z - 1}{z}\,, \quad Q^2 = xyzS\,. \tag{106}$$

(Note: The above variables corresponds to Q_t^2, x_t, y_t, described in Subsection 3.2.)

The differential cross section for the process $ep \to e\gamma X$, integrated over the photon emission angle inside a cone $\theta_\gamma \geq \pi - \theta_a$ reads

$$\frac{d^3\sigma}{dx\,dQ^2\,dz} = \alpha^3 P(z) \frac{1 + \left(1 - \frac{Q^2}{xzS}\right)^2}{xQ^4} [F_2(x,Q^2) - (1-\epsilon)F_L(x,Q^2)]\,, \tag{107}$$

where

$$P(z) = \frac{1+z^2}{1-z} \ln \frac{E_e^2 \theta_a^2}{m_e^2} - \frac{z}{1-z}, \tag{108}$$

and

$$\epsilon = \frac{2(1-y)}{1+(1-y)^2} = z \frac{2x\left(xz - \frac{Q^2}{S}\right)}{x^2 z^2 + \left(xz - \frac{Q^2}{S}\right)^2} \tag{109}$$

is the polarization of the virtual photon exchanged in the process. In the derivation of Eqs (107), (108) from the exact cross section for $ep \to e\gamma X$, all infrared and collinear finite terms have been neglected. Also terms of order $\mathcal{O}(m_e^2)$ are neglected and Eq. (108) is valid for not too small angle cutoffs, *i.e.* for $\theta_a \gg m_e/E_e$. Since we are interested in low Q^2 we restricted ourselves to pure photon exchange.

It is common to relate the structure functions to cross sections σ_T and σ_L for the scattering of transversely and longitudinally polarized photons:

$$\begin{aligned} F_2 &= \frac{Q^2}{4\pi^2 \alpha}(\sigma_L + \sigma_T), \\ F_L &= \frac{Q^2}{4\pi^2 \alpha}\sigma_L . \end{aligned} \tag{110}$$

In the following we are interested in the ratio

$$R = \frac{\sigma_L}{\sigma_T} . \tag{111}$$

Using these definitions, the cross section can be written in the form

$$\frac{d^3\sigma}{dx\, dQ^2\, dz} = \Gamma \sigma_T (1 + \epsilon R) \tag{112}$$

with

$$\Gamma = \frac{\alpha^2}{4\pi^2} P(z) \frac{1 + \left(1 - \frac{Q^2}{xzS}\right)^2}{xQ^2} . \tag{113}$$

The allowed range for z is $Q^2/xS \leq z \leq 1$. Since only photons with an energy above an experimental threshold $E_{\gamma,\min}$ can be observed, the upper limit of z is restricted:

$$z \leq z_{\max} = 1 - \frac{E_{\gamma,\min}}{E_e} . \tag{114}$$

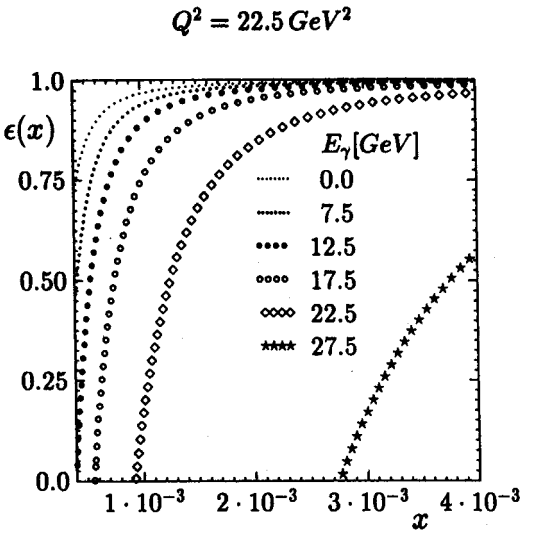

Fig. 19. Dependence of ϵ on x for various photon energies with fixed $Q^2 = 22.5\,\mathrm{GeV}^2$.

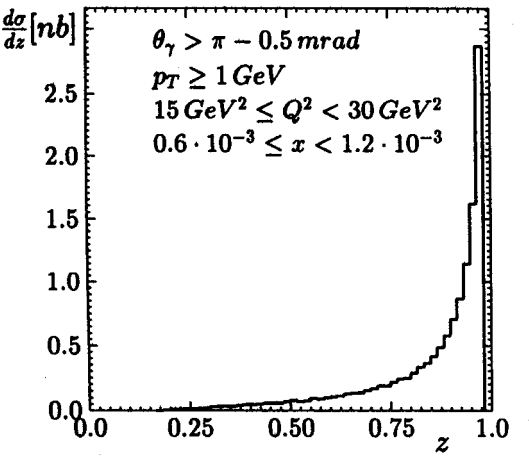

Fig. 20. The differential cross section $d\sigma/dz$ for initial state radiation with $\theta_\gamma \geq \pi - 0.5$ mrad integrated over $15\,\mathrm{GeV}^2 \leq Q^2 < 30\,\mathrm{GeV}^2$, $0.6 \cdot 10^{-3} \leq x < 1.2 \cdot 10^{-3}$. Additionally, a cut $p_T \geq 1\,\mathrm{GeV}$ was imposed.

Eq. (109) is a consequence of the rescaling Eq. (106) of the electronic variables to their true values due to photon emission. It is seen from this equation that at fixed x and Q^2, ϵ is a function of z and thus varies with the energy of the bremsstrahlung quanta. In Fig. 19, ϵ is shown as a function of x for various photon energies for a fixed $Q^2 = 22.5\,\mathrm{GeV}^2$. Here we used

$E_e = 30\,\mathrm{GeV}$ and $E_p = 820\,\mathrm{GeV}$. It is seen that at large x, very hard photons are needed to reach a sufficiently large variation of ϵ. Since the cross section decreases strongly with increasing photon energy, it will be more difficult to extract F_L at large x than at smaller x. The low photon energy cutoff $z \leq z_\mathrm{max}$ restricts the range of x where a measurement of F_L could be possible also from below by $x = Q^2/yzS \geq Q^2/z_\mathrm{max}S$.

Fig. 20 shows the spectrum of bremsstrahlung photons $d\sigma/dz$ for $\theta_a = 0.5$ mrad integrated over the range $6 \cdot 10^{-4} \leq x < 1.2 \cdot 10^{-3}$, $15\,\mathrm{GeV}^2 \leq Q^2 < 30\,\mathrm{GeV}^2$. These results were obtained from the Monte Carlo LESKO-F [29] which is based on the complete $\mathcal{O}(\alpha)$ cross section for $ep \to e\gamma X$ including also non-logarithmic terms. We checked that the collinear approximation of Eqs. (107), (108) indeed describes the cross section with excellent accuracy. With an integrated luminosity of $\int dt\mathcal{L} = 200\,\mathrm{pb}^{-1}$ one expects about 12,000 events with $\theta_\gamma \geq \pi - 0.5\,\mathrm{mrad}$ and $z \leq 0.75$ corresponding to $E_\gamma \geq 7.5\,\mathrm{GeV}$.

4.2. Statistical accuracy and systematic effects

In order to study the statistical and systematic accuracy for a possible R measurement which can be reached in a realistic experiment, we performed a Monte Carlo study with the help of the event generator LESKO-C [21]. This version of LESKO is based on the collinear approximation for initial state radiation as described above in Eq. (107). We assumed that the geometrical acceptance of the luminosity monitor is described by a constant value for $\theta_a = 0.5\,\mathrm{mrad}$. If not stated otherwise, we used the KMRS-B0 parametrizations for the parton distribution functions [62]. As input for the longitudinal structure function F_L we assumed $F_\mathrm{L} = R/(1+R) \cdot F_2$ (corresponding to Eq. (111)) with $R = 0.3$. Recent structure functions parametrizations predict R to be in the range $R \simeq 0.3 - 0.7$ [62, 91]. Statistical errors given below are for an integrated luminosity of $\int \mathcal{L}dt = 200\,\mathrm{pb}^{-1}$ corresponding to one year of running HERA with the design luminosity. The generated events were collected in a number of bins whose ranges have been chosen in view of the following considerations:

- A minimum energy for photons required in the luminosity counter of $E_\gamma \geq 7.5\,\mathrm{GeV}$ limits the range in x from below.
- The trigger rates require a minimum transverse momentum p_T. This limits x from below by $4p_\mathrm{T}^2/S$. A value of $p_\mathrm{T,min} = 3\,\mathrm{GeV}$ should be comfortable for both H1 and ZEUS. Also Q^2 is restricted from below by a minimum p_T.
- A precise determination of R can be expected only if a sufficient number of events can be collected over a wide range of ϵ which extends also to small values. As already discussed, this excludes large values of x.

- The bin sizes should be chosen such that the number of events is big enough and approximately equal in each bin.

We decided to consider 9 bins which cover in x the range from $6 \cdot 10^{-4}$ up to $2 \cdot 10^{-2}$ and in Q^2 from 15 GeV^2 to 120 GeV^2 (see Table I). In the photon energy, events have been collected in the following bins: $E_\gamma = (0-5.0)$ GeV, (7.5 ± 2.5) GeV, (12.5 ± 2.5) GeV, (17.5 ± 2.5) GeV, (22.5 ± 2.5) GeV, and (27.5 ± 2.5) GeV. The resulting central values for ϵ depend of course on x and Q^2. The first bin $(0-5)$ GeV is interpreted as containing those events which cannot be distinguished from non-radiative events and the value for ϵ for this bin is derived from Eq. (109) with $E_\gamma = 0$ (*i.e.* $z = 1$). Both in x and Q^2 the bin sizes are larger than 3σ of the detector resolution. Thus, migration of events from one bin into another should be small.

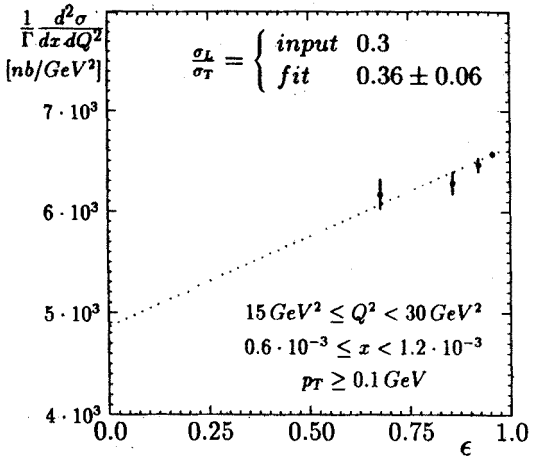

Fig. 21. Simulated measurement of $(d^2\sigma/dx\,dQ^2)/\Gamma$ and a linear fit to the Monte Carlo points for $0.6 \cdot 10^{-3} \le x < 1.2 \cdot 10^{-3}$, $15\,\text{GeV}^2 \le Q^2 < 30\,\text{GeV}^2$, and $p_T \ge 0.1$ GeV. Only statistical errors for $\int \mathcal{L}dt = 200\,\text{pb}^{-1}$ are shown.

Fig. 21 shows the results of our simulation in the bin $15\,\text{GeV}^2 \le Q^2 < 30\,\text{GeV}^2$ and $0.6 \cdot 10^{-3} \le x < 1.2 \cdot 10^{-3}$. The figure contains the simulated values for a measurement of $\sigma_T + \epsilon\sigma_L$ as a function of ϵ. The error bars represent the statistical accuracy. We also show in this figure the result of a linear fit which resulted in $R = 0.36 \pm 0.06$. We conclude from this that considering purely statistical errors, a measurement of R is indeed promising. However, this figure does not contain any systematic effect which we are going to discuss now.

The number of events N_i in a given bin i is determined by

$$N_i = \int_{\text{bin } i} dx\, dQ^2\, dz\, \Gamma(x, Q^2, z)(\sigma_T(x, Q^2) + \epsilon\sigma_L(x, Q^2)) . \tag{115}$$

In Fig. 21 it was assumed that this can be approximated by

$$N_i \simeq \Delta x\, \Delta Q^2\, \Delta z\, \Gamma(x_c, Q_c^2, z_c)(\sigma_T(x_c, Q_c^2) + \epsilon_c\sigma_L(x_c, Q_c^2)) , \tag{116}$$

where $\Gamma(\sigma_T + \epsilon\sigma_L)$ is evaluated at the bin center x_c, Q_c^2, ϵ_c. The error introduced by this approximation can be estimated if some sensible assumption about the dependence of the cross section on x and Q^2 is available. Since the variation of the cross section is dominated by the $1/Q^4$ behaviour due to the photon propagator, a reliable estimate can be obtained already without good knowledge of the structure functions. We calculated the error on $\Gamma(\sigma_T + \epsilon\sigma_L)$ resulting from the finite bin size by reducing Δx, ΔQ^2 and Δz until no dependence on the bin widths was observed anymore and corrected the results accordingly. The correction is typically of the order of 10 % (maximally 20 %). It was found that it is insensitive to variations of the input for parton distribution functions. Moreover, the correction depends only slightly on ϵ so that the cross section in each bin receives a correction but the fitted value of R is changed only very little. In order to estimate the systematic effect introduced by the fact that at the time when the correction is calculated the structure functions are not precisely known, we calculated the bin size correction using the parton distribution functions from Ref. [72] (set 1) whereas the events have always been generated with input from Ref. [62] (set B0).

In order to reach a high trigger efficiency and to reduce background from photoproduction and beam-gas as well as beam-wall events, it is necessary to apply a cut on the transverse momentum. In our Monte Carlo simulation we chose a cut of $p_T^e = p_T^h \geq p_{T,\min} = 3\,\text{GeV}$ which means also that we required always the scattered electron being observed in the detector. This kinematical restriction leads to an additional limit for ϵ. From $p_T = \sqrt{Q^2(1-y)}$ and using Eqs (106) and (109) one finds

$$Q^2 \geq p_{T,\min}^2 \frac{1 + \sqrt{1-\epsilon^2}}{\epsilon} . \tag{117}$$

This means that in bins with small ϵ the allowed phase space is restricted at small Q^2 and consequently the number of events is reduced. This would

lead to a steeper dependence of the cross section on ϵ and a larger value for the fitted R. By choosing a sensible extrapolation of the cross section to lower Q^2 this reduction can be corrected for. We applied this correction in the results to be presented below. The correction factor for each bin was determined from the ratio of events obtained in our Monte Carlo simulation with a cut $p_{T,min} = 0.1\,\text{GeV}$ and $p_{T,min} = 3.0\,\text{GeV}$. For $p_{T,min} = 0.1\,\text{GeV}$, the restriction Eq. (117) does not reduce the event number anymore in the bins we considered. The correction factor was in the worst case 2.1 (in the bin with smallest x, Q^2 and ϵ) but the typical magnitude was 1.1, and for $\epsilon \geq 0.9$ no effect is observed (see Eq. (117)). We checked, that this correction does not depend strongly on the input for the structure functions or the input value for R. Changing from MT-S parton distribution functions [92] to HMRS-E distributions [92], the correction changed by at most 3 %. One should keep in mind that HERA itself will provide information on the correct structure functions and we believe that at the time the analysis can be performed one will have a much better handle to determine this correction. Again, we applied the p_T cut correction to our simulated data, using DO-1 [72] for the determination of the correction but KMRS-B0 [62] for the simulation itself, introducing this way a possibility to estimate the corresponding systematic effect.

In Fig. 22 we show for the same bin as in Fig. 21 the results of the simulation but now including the corrections from bin size effects and from the p_T cut. The results including bin size and p_T cut corrections for the whole set of bins we have been considering are collected in Table I. Except of two bins, the values for the fitted R and for the input of $R = 0.3$ agree within statistical errors, showing that no large uncertainty is introduced by bin size and p_T cut corrections. We would like to stress that if the structure functions during such an analysis are precisely known, the latter uncertainty can be reduced and the agreement of the fitted R and the input one will be better.

The separation of σ_L from σ_T requires an efficient tagging and reconstruction of initial state radiation events. For this purpose one can use the luminosity monitor placed in both H1 and ZEUS experiments about 100 m downstream the electron direction. This photon calorimeter accepts photons emitted within an angular range of $0 - 0.5\,\text{mrad}$ [88]. A detailed discussion of the experimental aspects of the photon energy measurement is beyond the scope of this article, the reader interested in this subject we refer to Ref. [42]. We have found that the systematic effects introduced by the detector parameters and the quasi-elastic background are less than 0.2 in R. When data are well understood, most of the systematic effects could eventually be corrected for with the help of a detector Monte Carlo simulation and applied as a correction to the measured data.

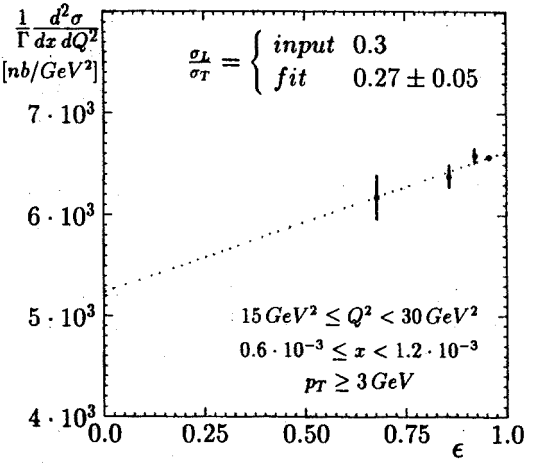

Fig. 22. As Fig. 21 but only events with $p_T \geq 3$ GeV were used and the data points have been corrected for the reduction of the event rates due to this cut and due to the finite bin size as described in the text.

TABLE I

Results of a linear fit to the Monte Carlo data including bin size and p_T corrections as described in the text.

$Q^2[\mathrm{GeV}^2]$	x	$R = \sigma_L/\sigma_T$
15 — 30	$0.6 \cdot 10^{-3}$ — $1.2 \cdot 10^{-3}$	0.27 ± 0.05
	$1.2 \cdot 10^{-3}$ — $2.0 \cdot 10^{-3}$	0.38 ± 0.24
	$2.0 \cdot 10^{-3}$ — $4.0 \cdot 10^{-3}$	0.24 ± 0.10
	$4.0 \cdot 10^{-3}$ — $8.0 \cdot 10^{-3}$	0.31 ± 0.18
30 — 60	$0.7 \cdot 10^{-3}$ — $2.0 \cdot 10^{-3}$	0.43 ± 0.08
	$2.0 \cdot 10^{-3}$ — $4.5 \cdot 10^{-3}$	0.42 ± 0.06
	$4.5 \cdot 10^{-3}$ — $1.0 \cdot 10^{-2}$	0.42 ± 0.16
60 — 120	$1.5 \cdot 10^{-3}$ — $5.0 \cdot 10^{-3}$	0.37 ± 0.06
	$5.0 \cdot 10^{-3}$ — $2.0 \cdot 10^{-2}$	0.29 ± 0.05

4.3. Conclusion

In conclusion, we have shown that the initial state radiation inelastic electron proton scattering should provide a means to measure R. We considered the kinematic range $15\,\mathrm{GeV}^2 \leq Q^2 < 120\,\mathrm{GeV}^2$ and $0.6 \cdot 10^{-3} \leq x < 2 \cdot 10^{-2}$ and found a statistical accuracy ranging from 0.05 to

0.25. Systematic shifts due to finite bin size, p_T cut, E_γ resolution, quasi-elastic background and E_γ miscalibration have been discussed and were found to be of the order of 0.2 in R.

Compared to the potential R measurement by reducing the beam energies [46], the proposed method should be considered as complementary. At the expense of larger uncertainties in the ϵ measurement, our method is insensitive to the precision of the luminosity measurement. It has in addition the advantage that the measurement can be performed in parallel to the planned physics program at HERA. We also hope that such a measurement will be possible in the future LEP/LHC experiment.

5. Summary

In this work we have discussed the problem of QED radiative corrections in deep inelastic $e^\pm p \to e^\pm X$ scattering. The discussion has been concentrated on the Monte Carlo treatment of QED radiative processes in the HERA experiments. In the first part of this article we have described *two Monte Carlo algorithms* for the simulation of the deep inelastic neutral current ($\gamma + Z$) electron proton scattering process including QED radiative effects. The older of them, which was constructed completely from the beginning for the HERA purpose, includes $\mathcal{O}(\alpha)$ *leptonic bremsstrahlung* and has been implemented in the program LESKO-F [29]. The other one describes *multiphoton radiation from the initial and final lepton states* basing on the Yennie–Frautschi–Suura exclusive exponentiation method. It was originally developed for the low angles Bhabha scattering at LEP/SLC [54] and then it has been adapted to the deep inelastic scattering process. The perturbative series of the Yennie–Frautschi–Suura type exponentiation formula includes $\mathcal{O}(\alpha)$ QED matrix elements which means that the emission of maximally one hard and many soft photons is well described. As was shown in Ref. [55], such a prescription apart from giving the proper soft photon limit and the full $\mathcal{O}(\alpha)$ hard photon description includes partly higher order leading corrections. Its QED precision is determined mainly by the second order subleading corrections, which seem to be unimportant at the HERA experimental accuracy level. This algorithm is a basis of the another Monte Carlo program for the HERA experiments, called LESKO-YFS[12] [30]. Both algorithms allow to generate weighted or unweighted (weight = 1) events. The latter, which represents the physical events, are obtained by the use of the rejection technique. In order to avoid contributions from the low

[12] Both programs, LESKO-F and LESKO-YFS, are put together into one Monte Carlo package for QED radiative processes at HERA, named LESKO-E [69], and can be chosen by setting an appropriate steering parameter option.

Q^2 region and restrict the event generation to the deep inelastic scattering domain, the lower cut on the hadronic transverse momentum, $p_{T,min}$, is imposed[13]. This means that events are always chosen from the range of $Q^2 > p^2_{T,min}$. Further restrictions of the kinematical domain can be introduced in terms of the hadronic (quark) x, Q^2, and y. The main variables used in the event generation are hadronic (quark) x and Q^2 for which radiative corrections are moderate and negative. This ensures the rejection rate to be relatively small. Radiation of photons from the initial and final electron state is generated with the help of the Sudakov-type variables which were adapted for the Monte Carlo purpose. All the variables needed to describe the final state particle are generated in several steps of the M.C. algorithm from probability distributions corresponding to a simplified differential cross section. For each simplification step an appropriate weight is calculated. As a result, the generated event is accompanied with the corresponding weight and it can be turned into the unweighted event by means of rejection. The presented algorithms are stable and efficient in the whole HERA kinematical domain.

We have also presented some numerical results from testing the above M.C. programs. The results of program LESKO-F were compared with analytical calculations in the leading logarithmic approximation. They agree within $\sim 5\%$ of accuracy what means that the major part of $\mathcal{O}(\alpha)$ QED corrections is properly included in the Monte Carlo. The differences should reveal the size of the subleading $\mathcal{O}(\alpha)$ contribution. The program was also compared with the equivalent M.C. generator HERACLES [36]. The results are presented in Ref. [26] and show a good agreement of these generators[14]. The new program LESKO-YFS we compared with LESKO-F. The results presented in this article show that the Yennie–Frautschi–Suura $\mathcal{O}(\alpha)$ exponentiation diminish negative corrections in the soft photon region (low y and large x) and increase slightly (up to a few per cent) positive corrections in the hard photon region (high y and low x) with respect to the $\mathcal{O}(\alpha)$ results. The differences between the YFS and $\mathcal{O}(\alpha)$ distributions decrease with increasing Q^2.

The programs LESKO-F and LESKO-YFS provide the hadronic final state at the parton level, *i.e.* in terms of the scattered quark and the unreacted proton remnant. For many practical reasons, however, it is desired to have the final state expressed fully in terms of physical particles. Therefore, we have developed an interface of the above programs to the hadronization routines. The interface, named FRANEQ [33], is based on the program

---

[13] The programs include also an option for lower Q^2 cut.

[14] HERACLES was shown to be in a good agreement with the $\mathcal{O}(\alpha)$ analytical calculation [26].

LEPTO 5.2 [34] and apart from hadronization it includes QCD radiative effects generated explicitly in terms of parton cascades. The quark and diquark fragmentation is covered by the Lund model implemented in the M.C. program JETSET 6.3 [35].

In the second part of this article we have discussed the problem of the unfolding of radiative corrections from the experimental data. We have presented *two novel* methods for reducing QED radiative effects at HERA: 1) by hard photon tagging and 2) by mixed electron and hadron measurement. In the first of them information from tagging events with hard photons close to the incident electrons is used to estimate the total size of the QED radiative correction. Hard photons emitted almost collinear with the initial electron beam are proposed to be detected in the luminosity measurement system. We have derived a simple formula in the leading logarithmic approximation which allows to make a good estimate of the Born cross section from two differential distributions: the fully inclusive cross section (from the electron measurement only) and one obtained after the rejection of the tagged hard photon events. The accuracy and efficiency of this method was tested by the use of the M.C. program LESKO-F. The important experimental systematic effects, as the photon energy smearing in the luminosity monitor (due to the E_γ resolution and the presence of the carbon filter) and the influence of the quasi-elastic radiative background, were also considered. We have proposed the effective way to deal with them in order to minimize their influence on the results. The quasi-elastic background which produces the major effect can be subtracted without measuring it by normalizing the tagged events at low y where the emission of the hard radiative deep inelastic photons is kinematically forbidden. We have shown that the proposed method can be applied at HERA in the kinematic region of $y_e > 0.1$, in particular at small x. The great advantage of this method is that it needs no assumption about the shape of the structure functions in the unmeasured region. In the second method radiative corrections are treated simultaneously with the unfolding of the experimental errors. The hard initial state radiation events are tagged and rejected from the event sample on the basis of the mismatch between the observed hadronic flow and that expected from the electron measurement. We have proposed three observables which can be used to identify the radiative events. The method was tested with the help of the program FRANEQ connected with LESKO-F. The experimental effects were simulated by smearing the kinematical variables according to the toy model of the detector. The results show that the remaining contributions to the acceptance corrections are small and to a large extent insensitive to the shape of the input structure functions. The efficiency of this method depends, however, on the angular coverage of the hadronic detector and the understanding of the resolution tails of the hadron energy measurement. It

may also be sensitive to the model dependent hadronization. Since, as it is evident from the above, the proposed methods have different sources of the systematic uncertainties it would be profitable to apply each of them to the data.

Finally, we have described the *new* method for determining the longitudinal structure function at HERA. We have shown that the emission of photons collinear with the incident electrons leads to the reduction of the effective beam energy which is sufficient to be used to measure the longitudinal structure function. The method was tested by the Monte Carlo simulations with the help of the programs LESKO-C [21] and LESKO-F. For the integrated luminosity of 200 pb^{-1} the statistical accuracy of the longitudinal and transverse cross section ratio R was found to be in the range of $\Delta R \simeq 0.05 - 0.25$ for $6 \cdot 10^{-4} \leq x < 2 \cdot 10^{-2}$ and $15\ \mathrm{GeV}^2 \leq Q^2 < 120\ \mathrm{GeV}^2$. The energy of the radiative photons was proposed to be measured in the luminosity monitor. The systematic shifts due to the E_γ resolution, the quasi-elastic radiative background, the E_γ miscalibration as well as the finite bin size and the p_T cut were also analysed. They were found to be of order of 0.2 in R. The presented method can be considered as complementary for the potential longitudinal structure function measurement by reducing the beam energies [46]. It may give larger uncertainty in the ϵ measurement but it is insensitive to the precision of the luminosity measurement. In addition, its great advantage is that the measurement can be performed in parallel to the planned physics program at HERA.

The author would like to thank dr. S. Jadach for the supervision and his constant support in this research, prof. K. Zalewski, prof. M. Zrałek and dr. Z. Wąs for critical reading of the manuscript. The fruitful collaboration with M.W. Krasny, M. Jeżabek and M. Przybycień is gratefully acknowledged. Useful discussions with K. Charchuła, K. Golec-Biernat, K. Piotrzkowski, E. Richter-Wąs, H. Spiesberger and Z. Wąs are appreciated. Finally, the author would like to express his gratitude for the hospitality of DESY in Hamburg, where parts of this work were done.

Appendix A

Matrix elements for lepton quark scattering

In the following we give explicit formulae for matrix elements of the neutral current lepton quark scattering process both at the Born level, *i.e.*

$$l(p_1) + q(q_1) \longrightarrow l(p_2) + q(q_2), \quad l = e^{\pm}, \tag{118}$$

and including single hard photon radiation from the lepton line, *i.e.*

$$l(p_1) + q(q_1) \longrightarrow l(p_2) + q(q_2) + \gamma(k), \quad l = e^{\pm}, \tag{119}$$

which are implemented in the algorithm of the program LESKO-F [29].

The differential cross section for the standard neutral current $lq \to lq$ scattering reads

$$D_{lq}(s,t) = \frac{\pi\alpha^2}{2s^2} \sum_{i,j=\gamma,Z} \left\{ [A_q^{ij}(s^2+u^2) + B_q^{ij}(s^2-u^2)] Q_l^2 P_i(t) P_j(t) \right\}, \quad (120)$$

where $s + t + u = 0$ (in the ultrarelativistic limit).

The matrix element for the process (119) which includes $\mathcal{O}(\alpha)$ hard photon bremsstrahlung from the initial and final lepton states can be written, following Ref. [95], as[15]

$$|\mathcal{M}_q^{\text{hard}}|^2 = |\mathcal{M}_q^{\text{hard}}|_{ml}^2 + |\mathcal{M}_q^{\text{hard}}|_{dp}^2, \quad (121)$$

where

$$|\mathcal{M}_q^{\text{hard}}|_{ml}^2 = \frac{\alpha^3}{8\pi^4} \sum_{i,j=\gamma,Z} \left\{ [A_q^{ij}(s^2+s_1^2+u^2+u_1^2) + B_q^{ij}(s^2+s_1^2-u^2-u_1^2)] \times Q_l^2 \frac{-t}{(kp_1)(kp_2)} P_i(t) P_j(t) \right\} \quad (122)$$

is the matrix element for massless spinors, and

$$|\mathcal{M}_q^{\text{hard}}|_{dp}^2 = -\frac{\alpha^3}{4\pi} \sum_{i,j=\gamma,Z} \left\{ [A_q^{ij}(s_1^2+u_1^2) + B_q^{ij}(s_1^2-u_1^2)] \frac{m_l^2}{(kp_1)^2} + [A_q^{ij}(s^2+u^2) + B_q^{ij}(s^2-u^2)] \frac{m_l^2}{(kp_2)^2} \right\} Q_l^2 P_i(t) P_j(t) \quad (123)$$

is the correction from the finite mass of spinors ($m_l \neq 0$).

The kinematical variables used in the above equations are defined as follows

$$\begin{aligned} s &= (p_1+q_1)^2, \quad t = (q_1-q_2)^2, \quad u = (p_1-q_2)^2, \\ s_1 &= (p_2+q_2)^2, \quad t_1 = (p_1-p_2)^2, \quad u_1 = (p_2-q_1)^2. \end{aligned} \quad (124)$$

They obey the relation

$$s + t + u + s_1 + t_1 + u_1 = 4(m_l^2 + m_q^2). \quad (125)$$

---

[15] In fact, Ref. [95] provides the matrix element for the Bhabha process, but it translates into the lepton quark scattering with rather minor changes.

The factors A_q^{ij} and B_q^{ij} in Eqs (120), (122) and (123) are combinations of the fermion–boson coupling constants for the electroweak neutral currents

$$A_q^{ij} = (\lambda_V^{l\,ij} - \epsilon\,\lambda_A^{l\,ij})\lambda_V^{q\,ij}\,,$$
$$B_q^{ij} = (\lambda_A^{l\,ij} - \epsilon\,\lambda_V^{l\,ij})\lambda_A^{q\,ij}\,, \tag{126}$$

where ϵ is the longitudinal spin polarization of the initial lepton while the quark is assumed to be unpolarized, and

$$\lambda_V^{f\,ij} = 2\,(v_f^i v_f^j - a_f^i a_f^j)\,,$$
$$\lambda_A^{f\,ij} = 2\,(v_f^i a_f^j - a_f^i v_f^j)\,. \tag{127}$$

The quantities

$$v_f^\gamma = -Q_f\,, \qquad a_f^\gamma = 0\,,$$
$$v_f^Z = \frac{I_f^3 - 2\,s_W^2 Q_f}{2\,s_W\,c_W}\,, \qquad a_f^Z = \frac{I_f^3}{2\,s_W\,c_W}\,, \tag{128}$$

are the neutral current coupling constants, where Q_f and I_f^3 are the electric charge and the weak isospin projection of the corresponding fermion $f_{L,R}$ ($f = l,\, q$), while $s_W = \sin\theta_W$, $c_W = \cos\theta_W$, where θ_W is the weak mixing angle (called also the Weinberg angle). In the minimal Standard Model of Electroweak Interactions [43]

$$s_W^2 = 1 - \frac{M_W^2}{M_Z^2}\,, \tag{129}$$

where M_W and M_Z are the masses of the weak intermediate bosons W and Z. Thus as an input set of parameters in calculation of electroweak coupling constants one can use α, M_W, M_Z. As long as M_W is not enough precisely known a better choice for the input parameters is the set α, G_μ, M_Z, where G_μ is the well measured muon decay constant. The weak coupling constants can be calculated now from the relation

$$s_W^2\,c_W^2 = \frac{\pi\alpha}{\sqrt{2}G_\mu M_Z^2}\,\frac{1}{1-\Delta r}\,, \tag{130}$$

where Δr includes higher order corrections to μ-decay. The programs LESKO-F and LESKO-YFS include options for the both input parameters sets. The formula for Δr is taken from Ref. [96]. It includes a mild

dependence on the top quark mass m_t and the Higgs mass $M_{\rm H}$ which must be taken as the additional input parameters.

The $P_{i,j}(t)$ in the formulae (120), (122) and (123) are the γ and Z^0 propagators,

$$P_\gamma(t) = \frac{1}{t(1+\Pi_{\gamma\gamma}(t))}\,,$$
$$P_Z(t) = \frac{1}{t-M_Z}\,, \tag{131}$$

where $\Pi_{\gamma\gamma}(t)$ is the vacuum polarization correction. The leptonic part of $\Pi_{\gamma\gamma}(t)$ is taken from Ref. [49] and the hadronic one is calculated using a dispersion relation from Ref. [50]. This takes into account the vacuum polarization corrections up to the leading $\mathcal{O}(\alpha^2)$ order, as pointed in Ref. [97].

Appendix B

Contributions to $\mathcal{O}(\alpha)$ YFS matrix element for lepton quark scattering

Contributions to the $\mathcal{O}(\alpha)$ matrix element of the Yennie–Frautschi–Suura type formula (52) located in the functions $\bar{\beta}$'s and defined in Eqs (57) and (58) reads as follows

$$D^{(0)}_{q,0} = \frac{t}{16t_p}\sum_{i,j=\gamma,Z}$$
$$\{A^{ij}_q(s^2+u^2+s_1^2+u_1^2) + B^{ij}_q(s^2-u^2+s_1^2-u_1^2)\}Q_l^2P_i(t)P_j(t)\,, \tag{132}$$

$$D^{(1)}_{q,1} = \frac{t}{16(kp_1)(kp_2)}\sum_{i,j=\gamma,Z}$$
$$\left\{A^{ij}_q\left[(s^2+u^2)\left(1-2\delta_t\frac{kp_1}{kp_2}\right)+(s_1^2+u_1^2)\left(1-2\delta_t\frac{kp_2}{kp_1}\right)\right]\right.$$
$$\left.+\,B^{ij}_q\left[(s^2-u^2)\left(1-2\delta_t\frac{kp_1}{kp_2}\right)+(s_1^2-u_1^2)\left(1-2\delta_t\frac{kp_2}{kp_1}\right)\right]\right\}Q_l^2P_i(t)P_j(t)\,,$$
$$\delta_t = \frac{m_l^2}{|\,t\,|}\,, \tag{133}$$

where the factors A^{ij}_q and B^{ij}_q as well as the γ and Z propagators $P_\gamma(t)$ and $P_Z(t)$ are given explicitly in Appendix A.

REFERENCES

[1] J.J. Thompson, *Phil. Mag.* **44**, 33 (1897).

[2] W.C. Roentgen, *Ueber eine neue Art von Strahlen (Vorlaeufige Mitteilung)*, Sitzungsberichte der physikalisch-medizinischen Gesellschaft zu Wuerzburg, 1896.

[3] J. Frank, G. Hertz, *Verhandl. Dert. Physik Ges.* **16**, 512 (1914).

[4] C.J. Davison, J. Germer, *Phys. Rev.* **30**, 707 (1927).

[5] R. Hofstadter, *Ann. Rev. Nucl. Sci.* **7**, 231 (1957).

[6] J.I. Friedmann, H. W. Kendall, *Ann. Rev. Nucl. Sci.* **22**, 203 (1972) and references therein; J.D. Bjorken, *Phys. Rev.* **179**, 1547 (1969). See also the published versions of the Nobel lectures: R.E. Taylor, *Rev. Mod. Phys.* **63**, 573 (1991); H.W. Kendall, *Rev. Mod. Phys.* **63**, 597 (1991); J.I. Friedman, *Rev. Mod. Phys.* **63**, 615 (1991).

[7] R.P. Feynmam, *Phys. Rev. Lett.* **23**, 1415 (1969).

[8] F.J. Hasert *et al.*, *Phys. Lett.***B1973**, 138 (1974); *Nucl. Phys.***B73**, 1 (1974).???

[9] D.J. Fox *et al.*, *Phys. Rev. Lett.* **33**, 1504 (1974).

[10] Proceedings of the HERA Workshop, Hamburg 1987, ed. P.D. Peccei, Vol. 1 and 2.

[11] Proceedings of the HERA Workshop "Physics at HERA", DESY Hamburg, Oct. 1991, ed. W. Buchmüller and G. Ingelman, Vol. 1, 2, 3, Hamburg, Apr. 1992.

[12] J. Bartels, DESY 90-153 (1990); E.M. Levin, DESY 91-110 (1991); B. Badełek, K. Charchuła, M. Krawczyk, J. Kwieciński, DESY 91-124 (1991); J. Feltesse, DPhPE 91-22, Saclay preprint (1991); in Proceedings of Nineteenth SLAC Summer Institute on Particle Physics "Lepton-Hadron Scattering", ed. J.F. Hawthorne, SLAC-REPORT-398, SLAC, Sept. 1992, page 155.

[13] J. Bartels, J. Feltesse, in [11], Vol. 1, page 131 and references therein.

[14] L. W. Mo, Y.S. Tsai, *Rev. Mod. Phys.* **41**, 205 (1969).

[15] M. Consoli, J. Dress, M. Greco, P. Dalpiaz, G. Gerhardt, in "Study on the Proton–Electron Storage Ring Project at HERA", report ECFA 80/42, DESY HERA 80/01, March 1980, page IV-88.

[16] D.Yu. Bardin, C. Burdik, P.Ch. Christova, T. Riemann, Dubna preprint E2-87-595, E2-88-682, and *Z. Phys.* **C42**, 679 (1989).

[17] D.Yu. Bardin, C. Burdik, P.Ch. Christova, T. Riemann, *Z. Phys.* **C44**, 149 (1989).

[18] M. Böhm, H. Spiesberger, *Nucl. Phys.* **B294**, 1081 (1987).

[19] M. Böhm, H. Spiesberger, *Nucl. Phys.* **B304**, 749 (1987).

[20] H. Spiesberger, in [10], Vol. 2, page 605.

[21] S. Jadach, MPI-PAE/PTh 75/86, preprint of MPI-München (1986).

[22] J. Kripfganz, H.-J. Möhring, *Z. Phys.* **C38**, 653 (1988).

[23] W. Beenemakker, F.A. Berends, W.L. van Neerven, Proceedings of the Ringberg Workshop on "Radiative Corrections for e^+e^- Collisions", ed J.H. Kühn, Ringberg 1989, page 3.

[24] J. Blümlein, *Z. Phys.* **47**, 89 (1990).

[25] W. Hollik, in [10], Vol. 2, page 579.
[26] H. Spiesberger *et al.*, in [11], Vol. 2, page 798.
[27] M.W. Krasny, DPhPE 91-21, Saclay preprint (1991) and in [11], Vol. 2, page 850.
[28] C. Kiesling, in [10], Vol. 2, page 653.
[29] S. Jadach, W. Płaczek, *Comput. Phys. Commun.* **72**, 221 (1992); 221; see also [11], Vol. 3, page 1330.
[30] S. Jadach, W. Płaczek, LESKO-YFS, in preparation; see also a short manual in the source code of the program.
[31] D.R. Yennie, S.C. Frautschi, H. Suura, *Ann. Phys.* (NY) **13**, 379 (1961).
[32] S. Jadach, *Acta Phys. Pol.* **B16**, 1007 (1987).
[33] W. Płaczek, *FRANEQ 2.0*, in [11], Vol. 3, page 1433; a short manual of the updated version of the program including multiphoton leptonic radiation, called FRANEQ 3.0, can be found in the source code.
[34] G. Ingelman, in [11], Vol. 3, page 1366 and references therein.
[35] T. Sjöstrand, *Comp. Phys. Commun.* **39**, 347 (1986); T. Sjöstrand, M. Bengtsson, *Comp. Phys. Commun.* **43**, 367 (1987).
[36] A. Kwiatkowski, H.-J. Möhring, H. Spiesberger, *Comp. Phys. Commun.* **69**, 155 (1992); see also [11], Vol. 3, page 1294.
[37] H. Anlauf, H.D. Dahmen, P. Manakos, T. Mannel, T. Ohl, *Comp. Phys. Commun.* **70**, 97 (1992).
[38] G.P. Lepage, *VEGAS, J. Comput. Phys.* **27**, 192 (1978).
[39] S. Jadach, M. Jeżabek, W. Płaczek, *Phys. Lett.* **B248**, 417 (1990).
[40] W. Płaczek, M. Przybycień, TPJU 3/92, Jagellonian Univ. preprint (1992) and in [11], Vol. 2, page 891.
[41] M.W. Krasny, W. Płaczek, in [11], Vol. 2, page 862.
[42] M. W. Krasny, W. Płaczek, H. Spiesberger, *Z. Phys.* **C53**, 687 (1992); DESY 91-117 (1991) and DPhPE 91-11 (1991) preprints; see also [11], Vol. 1, page 171.
[43] S. Glashow, *Nucl. Phys.* **22**, 579 (1961); A. Salam, in *Elementary Particle Theory*, ed. H. Svartholm, Almquist, Stockholm 1968; S. Weinberg, *Phys. Rev. Lett.* **19**, 1264 (1967).
[44] A. Sirlin, *Phys. Rev.* **D22**, 971 (1980).
[45] C.G. Callan, D.G. Gross, *Phys. Rev. Lett.* **21**, 311 (1968); *Phys. Rev. Lett.* **22**, 156 (1969).
[46] A.M. Cooper-Sarkar, G. Ingelman, K.R. Long, R.G. Roberts, D.H. Saxon, *Z. Phys.* **39**, 281 (1988) and in [10], Vol. 1, page 231; A.M. Cooper-Sarkar, R.C.E. Devenish, M. Lancaster, in [11], Vol. 1, page 155.
[47] A. de Rújula, R. Petronzio, A. Savoy-Navarro, *Nucl. Phys.* **154**, 394 (1979).
[48] J. Kripfganz, P. Perlt, *Z. Phys.* **41**, 319 (1988).
[49] G. Burgers, W. Hollik, in: *Polarization at LEP*, CERN 88-06, eds G. Alexander *et al.*, Vol. 1, page 136.
[50] H. Burkhardt, F. Jegerlehner, G. Penso, C. Verzegnassi, in *Polarization at LEP*, CERN 88-06, eds G. Alexander *et al.*, Vol. 1, page 145 and *Z. Phys.* **43**, 497 (1989).

[51] M. Skrzypek, *Acta Phys. Pol.* **B23**, 135 (1992).
[52] J. Kripfganz, H.-J. Möhring, H. Spiesberger, *Z. Phys.* **49**, 501 (1991).
[53] S. Jadach, B.F.L. Ward, *Comp. Phys. Commun.* **56**, 351 (1990).
[54] S. Jadach, E. Richter-Wąs, B.F.L. Ward, Z. Wąs, CERN-TH.6230/91 (1991) and *Comp. Phys. Commun.* **70**, 305 (1992).
[55] S. Jadach, E. Richter-Wąs, B.F.L. Ward, Z. Wąs, *Phys. Lett.***B260**, 438 (1991).
[56] F. James, *Rep. Prog. Phys.* **43**, 1145 (1980).
[57] R. Kleiss, CERN-TH.5732/90, May 1990.
[58] F. James, *Comp. Phys. Commun.* **60**, 329 (1990); G. Marsaglia, A. Zaman, W.-W. Tsang, *Stat. Prob. Lett.* **9**, 35 (1990).
[59] P. L'Ecuyer, *Comm. ACM* **31**, 742 (1988).
[60] K. Charchuła, DESY 91-093 and *Comp. Phys. Commun.* **69**, 360 (1992).
[61] S. Jadach, *The two-dimensional M.C. sampler VESKO2*, the source code, to be obtained from the author.
[62] J. Kwieciński, A. Martin, R. Roberts, J. Stirling, *Phys. Rev.* **D42**, 3645 (1990).
[63] S. Jadach, B.F.L. Ward, Exclusive exponentiation in the Monte Carlo Yennie-Frautschi-Suura approach, in Proc. Sussex University Conference "Elecroweak Physics", eds N. Dombey and F. Boundjema, Plenum Publ. Co., London 1989.
[64] S. Jadach, MPI-PAE/PTh 6/87, Jan. 1987.
[65] S. Jadach, B.F.L. Ward, *Phys. Rev.* **D38**, 2897 (1988).
[66] S. Jadach, B.F.L. Ward, *Phys. Rev.* **D40**, 3582 (1989).
[67] S. Jadach, E. Richter-Wąs, B.F.L. Ward, Z. Wąs, *Phys. Lett.* **B268**, 253 (1991); preprint CERN-TH.6118/91 (1991).
[68] V.V. Sudakov, *Zh. Eksp. Teor. Fiz.* **30**, (1956); *Sov. Phys. JETP* **3**, 115 (1956).
[69] S. Jadach, W. Płaczek, The Monte Carlo package LESKO-E for deep inelastic electron proton neutral current scattering at HERA including QED radiative processes, in preparation; see also the brief manual in the source code (to be obtained from the authors).
[70] S. Jadach, E. Richter-Wąs, B.F.L. Ward, Z. Wąs, *Phys. Lett.* **B253**, 469 (1991).
[71] Z. Wąs, S. Jadach, CERN-TH.6159/91 (1991).
[72] D.W. Duke, J.F. Owens, *Phys. Rev.* **D30**, 49 (1984).
[73] S. Jadach, W. Płaczek, E. Richter-Wąs, B.F.L. Ward, Z. Wąs, QED corrections to small angle Bhabha and quark-electron scattering, in Proceedings of "1992 Zeuthen Workshop on Elementary Particle Theory", Apr. 1992, Nucl. Phys. **B**, (Proc. Supl.) 29A, 285 (1992); Jagellonian Univ. preprint TPJU-14/92 (1992).
[74] D.Yu. Bardin, C. Burdik, P.Ch. Christova, T. Riemann, Dubna preprint E2-88-682 (1988).
[75] N.M. Shumeiko, *Yad. Fiz.* **29**, 1571 (1979).
[76] G. Bernardi, W. Hildesheim, in [11], Vol. 1, page 79.
[77] G. Ingelman, K. Meier, B.R. Webber, in [11], Vol. 1, page 255 and references therein.
[78] G. Grindhammer, in [11], Vol. 3, page 1153 and references therein.
[79] N. Magnussen *et al.*, in [11], Vol. 3, page 1167.
[80] M. Bengtsson, G. Ingelman, T. Sjöstrand, in [10], Vol. 1, page 141.

[81] B. Anderson, G. Gustafson, G. Ingelman, T. Sjöstrand, *Phys. Rep.* **97**, 31 (1983).
[82] G.A. Schuler, H. Spiesberger, DJANGO 1.0, in [11], Vol. 3, page 1419.
[83] G. Marchesini, B.R. Webber, M.H. Seymour, G. Abbiendi, L. Stanco, I.G. Knowles, *Comput. Phys. Commun.* **67**, 465 (1992); see also B.R. Webber, in [11], Vol. 3, page 1354.
[84] T. Ohl, DESY 92-097 preprint (1992).
[85] G. Levman, in [11], Vol. 2, page 876.
[86] V.N. Gribov, L.N. Lipatov, *Sov. J. Nucl. Phys.* **15**, 438 (1972); *Sov. J. Nucl. Phys.* **15**, 675 (1972); G. Altarelli, G. Parisi, *Nucl. Phys.* **B126**, 298 (1977); Yu.L. Dokshitzer, *Sov. Phys. JETP* **46**, 671 (1977).
[87] L. Suszycki *et al.*, in [10], Vol. 2, page 503.
[88] H1 Collaboration, H1 Technical Report, TR-113 (1987). ZEUS Collaboration, The ZEUS Detector, Status Report 1989.
[89] M. Przybycień, private communications.
[90] A. Blondel, F. Jacquet, DESY 79/48, page 391.
[91] J. Morfin, Wu-Ki Tung, FERMILAB-Pub-90/74.
[92] P.N. Harriman, A.D. Martin, W.J. Stirling, R.G. Roberts, *Phys. Rev.* **D42**, 798 (1990).
[93] M.W. Krasny, W. Płaczek, in preparation.
[94] D.Yu. Bardin, J. Ciborowski, in [11], Vol. 2, page 885.
[95] G. Burgers *et al.*, CALKUL Collaboration, *Nucl. Phys.* **B206**, 61 (1982).
[96] W. Hollik, MPI-Ph/92-2, Jan. 1992; see also W. Hollik *et al.*, in [11], Vol. 2, page 923.
[97] W. Beenakker, F.A. Berends, S.C. van der Marck, *Nucl. Phys.* **B355**, 281 (1991).